Study of Rotating Flows and Heat Transfer for Casson Nanofluid under Uniform Magnetic Field

By

Ume Hani

(Fall 2016 CS&E 00000170418)

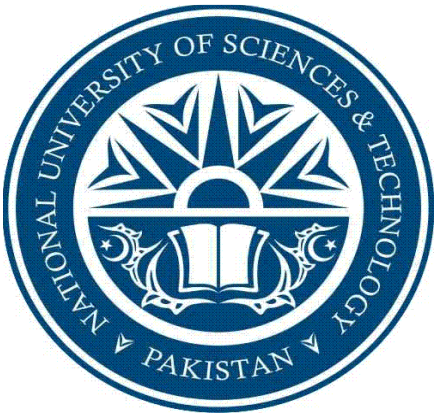

A thesis submitted in partial fulfillment of the requirements
for the degree of Master of Science in Computational Science and Engineering

Supervised by

Dr. Junaid Ahmad Khan

Research Centre for Modeling and Simulation,
National University of Sciences and Technology,
Islamabad, Pakistan

January 2020

Dedication

To my dearest Parents,

Acknowledgment

First and foremost, I would like to thank Allah Almighty, the author of knowledge and wisdom, for His countless blessings. I am thankful to Him for blessing me with so many precious people who assisted me throughout this journey.

I am extremely grateful and wish to convey my sincere gratitude to my respected supervisor Dr. Junaid Ahmad Khan, Assistant Professor RCMS, NUST, for his continuous supervision throughout my MS degree and research work. His trust in me kept me focused and determined. I would like to thank him for his constant assistance, for the invaluable guidance he provided me whenever I need and the tremendous efforts to offer every possible help to finish this thesis.

I would like to thank Dr. Rizwan Riaz principal RCMS, NUST, for providing us a better environment and all the learning facilities, which helped in completion of this research work. I would like to present cordial gratitude to my respected GEC members Dr. Absaar Ul Jabbar, Dr. Ammar Mushtaq and Dr. Israr Ud Din. They all always provided me sincere guidance and constant support with honest advices.

In the end I want to pay my deepest gratitude to all the faculty members, lab engineers and other staff members of RCMS, NUST, for having the positive and supportive role in this beautiful journey of my MS.

Contents

List of Symbols

ϕ	Concentration of Nanoparticles
β	Casson Parameter
Bi	Biot number
C_f	Skin friction coefficient
Pr	Prandtl number
Sc	Schmidt number
Sh	Sherwood number
Nt	Thermophoresis
Nu	Nusselt number
Nb	Brownian Motion
M	Hartmann number

List of Tables

List of Figures

Abstract

A fluid for which stress isn't linearly related to deformation rate is termed as a non-Newtonian fluid. Such fluids help us comprehend the widespread variety of fluids that occur in the physical world. Many researchers explored non-Newtonian fluids via Casson model which is preferred due to its wide-ranging applications. This work includes a brief background of the research undertaken in this thesis. Dimensionless numbers and their significance are described briefly. Some important concepts employed in the thesis are also explained. Further we have described the basic equations of incompressible fluids and models for transport of nanofluids. Numerical technique is also discussed in detail. Heat transfer and Skin friction coefficient effects on a Casson Nanofluid flow rotating on a stretching disk is subjected to convective heating are discussed. A convenient routine bvp4c of MATLAB and Keller box method are invoked to find graphical and numerical solutions. Casson parameter β and magnetic parameter M have very small effect on radial component of velocity. Heat transfer is decreasing against high Prandtl number. There is non-linear relationship between the skin friction coefficient and volume fraction of nanoparticles. Thermal boundary layer decreases with increase in thermophoresis parameter. At high thermophoresis parameter there is a decrease in heat transfer rate. The stretching forces and magnetic forces balance each other. In the end the summary of conclusions and future work is described.

Chapter 1 **Introduction**

The flows involving non-Newtonian fluids have wide spectrum of applications in industrial processes such as synthetic fibers, polymer solutions, paper production etc. A huge variety of biological as well as industrial fluids show non-Newtonian behavior, for example, blood, printer ink, ketchup, slurries and grease etc.

Fluids which do not adhere to Newton's law of viscosity are classified as non-Newtonian fluids. For these fluids, shear stress and deformation rate cannot be linked linearly. Under stresses, such fluids change their viscosity with varying strain rate.

Since there is no linear relation between stress and deformation rate, a single model cannot be used to explain non-Newtonian fluids. Researchers have developed many multiple models to study non-Newtonian fluids. Some widely used models are power-law model, Casson Model, Bingham Model, Bird-Carreau model, Cross-Power law model, Herschel-Bulkey model, second-grade model etc. While quietly accepted and utilized model is the Casson model.

Nanofluids are the modern generation heat transfer fluids which holds peculiar heat transfer even at very low particle concentrations. First of all, Masuda et al. [1] discovered that both viscosity and thermal conductivity can be enhanced by dispersing nanometer-sized metallic particles in the fluid. Choi and Eastman [2] combined the conventional heat transfer fluids with nanometer sized metallic particles and observed a significant increase in the thermal conductivity of the resulting liquid. In another paper, Eastman et al. [3] discussed an abnormal increase in the thermal conductivity of ethylene glycol based nanofluids. Buongiorno [4] studied the convective transport phenomena in nanofluids and concluded that out of the seven slip mechanisms namely inertia, Brownian diffusion, thermophoresis, diffusiophoresis, Magnus effect, fluid drainage and

gravity settlings only Brownian motion and thermophoresis diffusion of nanoparticles contribute to the massive increase in the absolute thermal conductivity of the liquids. He also developed a mathematical model for nanofluid flow which incorporates the simultaneous effects of Brownian motion and thermophoresis diffusion of nanoparticles. Later Tiwari and Das [5] presented a mathematical model for nanofluids by accounting the solid volume fraction of two phase mixture.

MHD fluid flow along with heat transfer has wide significance due to its versatile range of applications. These applications can be noticed in MHD power generator, aerospace technology, turbo-machinery, heat exchanger, MHD pumps, underground cable, electronic devices, telecommunication, petroleum and chemical engineering.

1.1 Literature survey

The rotational flow problem for stretching plate was taken in account by Wang [6] first time. His study has a pivotal usage in geophysical flows. Wang extracted the similarity solution for Naiver-Stroke equations. Lambda is the significant parameter of his work which determines the ratio of rotation to the stretching rate. Rajeswari and Nath [7] further extended Wang's idea by working on the unsteady situation. Afterward the numerical solution for unsteady rotational flow for a stretching sheet was given by Nazar et al. [8] and he also gave the asymptotic result for steady state. The asymptotic solution shows a linear transition from the initially unsteady fluid flow to the steady state of flow. Hayat et al. [9] found the analytical solution for rotational flow over shrinking surface by electrically conducting second grade fluid. Abbas et al. [7] worked further on Nazar et al. [10] problem by introducing the magnetic field effects. Two different phases for the symmetrically rotating viscous flow were discovered by Batchelor [11] those flows in which the flow above the plane from the origin where the fluid at infinity is rotating like

a rigid body and Bödewadt's problem lies in this family. The part two of the problem deals with the finite distance where the rotational fluid flow behaves as rigid body between two planes. Physically realistic solutions were introduced by Roger and Lance [12] and McLeod [13] when resolved the Batchelor's problem and found that only at infinity when rotation of fluid is on the same pattern as that of the disk. The classical Bödewadt flow of boundary layer with radially stretching disk was studied by Turkyilmazoglu [14]. He concluded that the radially stretched phenomena has the ability to decreases the boundary layer and increases the heat transfer coefficient. The recent progress on rotational fluid flows can be seen in References [15–26].

At present time researchers have keen interest in Casson due to its wide applications in industry e.g. the manufacturing of pharmaceutical products, coal in water, china clay, paints, synthetic lubricants, and biological fluids such as synovial fluids etc. The flow of Casson nanofluid for vertical exponentially stretching cylinder was studied by Malik and others [27]. Sarojamma and Vendabai [28] extended the work of Malik and others [28] by introducing the magnetic effects on the boundary layer flow of a Casson nanofluid for a vertical exponentially stretching cylinder. The fluid flow of Casson nanofluid with viscous dissipation effects and influence of convective conditions was presented by Hussain and others [29]. Sathies kumar and Gangadhar [30] studied the effects of MHD slip flow of Casson fluid of a chemical reaction with a stretching sheet for heat and mass transfer. A model for Casson nanofluid flow past over a nonlinearly stretching sheet considering magnetic field effects was presented by Mustafa and Junaid [31]. The current trends of this research area can be seen in References

[32-47].

The magneto nano-liquids have remarkable importance in biomedical field. These liquids have vast applications in stomach medicines, sterilizing devices, biomaterials for injury treatments etc. The applied magnetic field is considered one of the best methods to utilize the electrically conducting nano-liquids to get the finest quality products in industrial engineering. Various studies have been carried out in past to examine the importance of MHD nanofluid. The recent progress on MHD fluid flows can be seen in References [48–55].

1.1.1 Problem Statement

Bodewadt flow is a type of rotating flow with a wide range of applications. Literature survey showed no research articles of Bodewadt flow under uniform magnetic field. Therefore, an investigation of Bodewadt flow for Non-Newtonian nanofluid under uniform magnetic field is required to understand the flow behavior.

1.2 Research objectives

Based on the above problem statement and literature survey the main objectives of the research are as below:

1. To formulate mathematical model for Bodewadt flow for Casson nanofluid.
2. To study the effects of various Non-dimensional parameters on rotating flow.
3. To study the behavior of skin friction and heat transfer rate.
4. To provide solutions by different numerical approaches namely Keller box method and bvp4c package.

1.3 Some dimensionless numbers

1.3.1 Reynolds number

Reynolds numbers (Re) is used to predict whether the flow is laminar or turbulent. Mathematically, the ratio of inertial forces to viscous forces defines Reynolds number, given by:

$$Re = \frac{\rho v L}{\mu} = \frac{vL}{\nu} \tag{1.1}$$

where L is the characteristic length, $\nu = \mu/\rho$ is termed as kinematic viscosity, μ is the dynamic viscosity of the fluid and ρ is the density of the fluid. At low Reynolds number, viscous forces relatively dominate thereby producing laminar flow. On the other hand, inertial forces dominate at high Reynolds number and thus initiate turbulence in fluid flow.

1.3.2 Prandtl number

Prandtl number (Pr) is used to determine heat transfer between a moving fluid and a solid surface. Mathematically, it is the ratio of momentum diffusion to thermal diffusion, represented as:

$$Pr = \frac{\nu}{\alpha} = \frac{c_p \mu}{\kappa}, \tag{1.2}$$

where $\alpha = \kappa/\rho c_p$ denotes the thermal diffusivity in which κ is thermal conductivity and c_p represents the specific heat capacity.

1.3.3 Nusselt number

The ratio of convective heat transfer to conductive heat transfer defines Nusselt number. Mathematically:

$$Nu = \frac{h}{\kappa/L}, \tag{1.3}$$

where h is the convective heat transfer coefficient.

1.3.4 Schmidt number

The Schmidt number is defined as the ratio of momentum diffusivity (kinematic viscosity) and mass diffusivity, and is used to characterize fluid flows in which there are simultaneous momentum and mass diffusion convection processes. The Schmidt number describes the mass momentum transfer, and the equations can be seen below:

$$Sc = \frac{\nu}{D} = \frac{\mu}{\rho D} \tag{1.4}$$

D is the mass diffusivity.

1.3.5 Biot number

Biot number analyzes the interaction between conduction in a solid and convection at the solid's surface. Mathematically,

$$Bi = \frac{h}{k\sqrt{\nu/U}}, \tag{1.5}$$

Where h is a convective heat transfer coefficient , k is the thermal conductivity and U is the horizontal velocity of the plate.

1.3.6 Hartmann number

It is a parameter of prime importance when the flow is exposed to a transverse magnetic field being applied externally. Mathematically, it is the ratio of electromagnetic force to the viscous force, represented as:

$$M = \sqrt{\frac{\sigma B^2}{\rho U}}, \tag{1.6}$$

where σ denotes electrical conductivity, B is magnetic field intensity and U is horizontal velocity of the plate.

1.3.7 Sherwood Number

Sherwood numbers represent the effectiveness of heat and mass convection at the surface. Mathematically it is written as:

$$Sh = \frac{h}{D/L} \tag{1.7}$$

L is a characteristic length and D is the mass diffusivity.

1.3.8 Thermophoresis

Thermophoresis is a phenomenon observed in mixtures of mobile particles where the different particle types exhibit different responses to the force of a temperature gradient.

1.3.9 Brownian motion

This motion is named after the botanist Robert Brown, who first described the phenomenon in 1827. It is the random motion of particles suspended in a fluid resulting from their collision with the fast-moving molecules in the fluid.

1.4 Preliminary concepts

1.4.1 Boundary layer

Boundary layer refers to the layer of fluid surrounding the boundary where the effect of the viscosity is present. Two important types of boundary layers are discussed below:

1.4.2 Momentum boundary layer

When fluid particles come in contact with a solid surface, they exhibit a zero velocity in order to adhere to the no-slip condition. These fluid particles impact the particles of the adjacent fluid layer and it consequentially influences the next layer fluid particles. This slowing of velocity goes on till a considerable distance from the flat surface is achieved where the retardation effect becomes negligible. In the boundary layer, fluid velocity varies from zero to $0.99U_{\infty}$, where U_{∞} represents free stream velocity.

1.4.3 Thermal boundary layer

Thermal boundary layer forms when there is a temperature difference between the fluid flow and the surface across which the flow is flowing. This is the region where the temperature varies along $y-$ direction i.e. normal to the surface (as in Fig. 1.1).

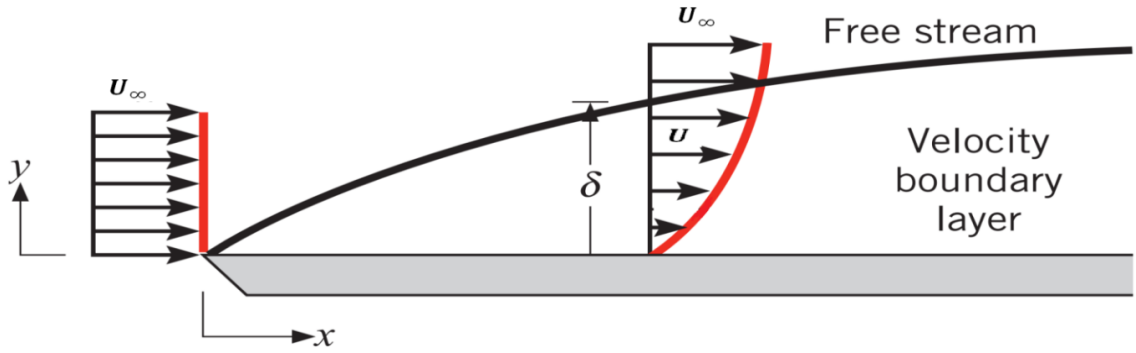

Figure 1.1: Boundary layer schematic

1.4.4 Casson fluid

In order to examine the properties of flow and heat transfer many rheological models have been put forward. There is type of non-Newtonian fluid known as Casson fluid. This model is prominent for many materials. Some suspension flows are also closely related to this model.

Casson fluid is a shear thinning liquid and exhibits yield stress. It is assumed that this fluid has an infinite viscosity at zero rate of shear, a yield stress below which no flow occurs, and a zero viscosity at an infinite rate of shear, i.e., if a shear stress less than the yield stress is applied to the fluid, it behaves like a solid, whereas if a shear stress greater than yield stress is applied, it starts to move.

Casson fluid is of the type as syrups, paper pulp in water, glues, emulsions, soaps, sugar solution, latex paints, sand in water, shampoos, custard etc.

Human blood can also be treated as Casson fluid. Due to the presence of several substances like, protein, fibrinogen, and globulin in aqueous base plasma, human red blood cells can form a

chainlike structure, known as aggregates or rouleaux. If the rouleaux behave like a plastic solid, then there exists a yield stress that can be identified with the constant yield stress in Casson fluid. The rheological equation of state for an isotropic and incompressible flow of a Casson fluid is given by:

$$\tau_{ij} = \begin{cases} 2\left(\mu_B + \frac{p_y}{\sqrt{2\pi}}\right)e_{ij}, & \pi > \pi_c \\ 2\left(\mu_B + \frac{p_y}{\sqrt{2\pi_c}}\right)e_{ij}, & \pi < \pi_c \end{cases} \tag{1.8}$$

Where $\pi = e_{ij}e_{ij}$ and e_{ij} are the deformation rate of (i, j)th component, π is the product of deformation rate with itself. π_c is the critical value of π, μ_B is the plastic dynamic viscosity of Casson fluid and p_y is the yield stress of Casson fluid.

Chapter 2 Mathematical Modeling and Numerical Methodology.

The governing equations of fluid flow motion are derived from the fundamental principles of conservation of mass, momentum and energy. The relation between shear stress and strain rate through the rheological properties of the fluid can be of different forms. Here are the basic boundary layer equations which will be used in the later chapter of this dissertation.

2.1 Laws of Conservation

2.1.1 Law of Conservation of Mass

Physical principle Mass can be neither created nor destroyed.

$$\frac{\partial \rho}{\partial t} + \boldsymbol{\nabla}.(\rho \boldsymbol{V}) = 0 \tag{2.1.1}$$

ρ is the fluid density, t is the time, $\boldsymbol{\nabla}$ is the divergence and $\boldsymbol{V} = [u, v, w]$ is the velocity vector.

The above equation (2.1.1) is called the **Continuity equation** and describes the transport of some quantity.

2.1.2 Law of Conservation of Momentum

Physical principle Force = time rate of change of momentum.

As the fluid flows through some material or body it comprises two types of forces in this situation:

Body forces: gravity, electromagnetic forces or any other forces.

Surface forces: pressure and shear stress acting on the surface of material/body.

Hence mathematical form of momentum equation is given as:

$$\rho \frac{D\boldsymbol{V}}{Dt} = -\boldsymbol{\nabla} P + \boldsymbol{\nabla}.\tau + \rho \boldsymbol{g} \tag{2.1.2}$$

$\frac{D\boldsymbol{V}}{Dt}$ is the total derivative, P is the pressure, τ is the shear stress and $\boldsymbol{g}$ is the gravitational force vector.

The total derivative can also be represented as:

$$\frac{D\boldsymbol{V}}{Dt} = \frac{\partial}{\partial t} + (\boldsymbol{V}.\nabla)$$

Therefore, we can write equation (2.1.2) as:

$$\rho \left(\frac{\partial \boldsymbol{V}}{\partial t} + (\boldsymbol{V}.\nabla)\boldsymbol{V} \right) = -\boldsymbol{\nabla} P + \boldsymbol{\nabla}.\tau + \rho \boldsymbol{g} \tag{2.1.3}$$

The momentum equations for viscous flow are called *as Navier-Strokes equation.*

2.1.3 Law of Conservation of Energy

Law of conservation of energy states that the rate of increase of energy of fluid particle is equal to net rate of heat added to the fluid particle plus net rate of work done on the fluid particle.

Physical principle Energy can be neither created nor be destroyed.

Mathematically it can be written as:

$$\rho c_p \frac{DT}{Dt} = -\Delta . \boldsymbol{q} + \Phi \tag{2.1.4}$$

c_p, $\boldsymbol{q}$ are the specific heat and heat flux of the fluid flow respectively while Φ is the viscous dissipation.

2.2 Magneto hydrodynamic (MHD) Flow

This shows how a magnetic field influences the conductive fluid flows.

When we make analysis of a MHD fluid flow the momentum equation becomes:

$$\rho\left(\frac{\partial V}{\partial t} + (\boldsymbol{V}.\boldsymbol{\nabla})\right)\boldsymbol{V} = -\boldsymbol{\nabla}P + \boldsymbol{\nabla}.\tau + j \times B \tag{2.2.1}$$

Where j is the current density and $\boldsymbol{B}$ is magnetic field and $j \times \boldsymbol{B}$ is the Lorentz force. $\boldsymbol{B} = (0, 0, B)$.

$j = \sigma E'$ and $E' = E + (\boldsymbol{V} \times \boldsymbol{B}) = \sigma (\boldsymbol{V} \times \boldsymbol{B}) \times \boldsymbol{B}$. When fluid is moving with respect to external magnetic and electric field at velocity **V** external Electric field is zero. Therefore, we have $E' = (\boldsymbol{V} \times \boldsymbol{B})$. Hence we can write:

$$E' = \sigma (\boldsymbol{V} \times \boldsymbol{B}) \times \boldsymbol{B} \tag{2.2.2}$$

and

$$\boldsymbol{V} \times \boldsymbol{B} = \begin{vmatrix} i & j & k \\ u & v & w \\ 0 & 0 & B_o \end{vmatrix} = ivB_o - juB_o \tag{2.2.3}$$

Therefore, we can write

$$(\boldsymbol{V} \times \boldsymbol{B}) \times \boldsymbol{B} = \begin{vmatrix} i & j & k \\ vB_o & -uB_o & 0 \\ 0 & 0 & B_o \end{vmatrix} = -iuB_o^2 - jvB_o^2 \tag{2.2.4}$$

Hence x-component $= -uB_o^2$, y-component $= -vB_o^2$ and z-component $= 0$.

Hence above mentioned equations and derivations presented a detailed review of our Mathematical model which is considered in this dissertation.

2.3 Mathematical Models for Nanofluid Transport

Moreover, following are the two nanofluid transport models which we have taken

into account for the calculation of results.

i. Homogenous Model

ii. Non-Homogenous Model

2.3.1 Homogenous Model

It is also called as Tiwari and Das Model. It is Single-Phase homogenous model without concentration equation model.

For steady incompressible flow of Nano fluid, the continuity, momentum and energy equations are given below:

$$\nabla . \boldsymbol{V} = 0 \tag{2.3.1}$$

$$\rho_{nf}(\boldsymbol{V}.\nabla)\boldsymbol{V} = -\nabla p + \mu_{nf}\nabla^2\boldsymbol{V} \tag{2.3.2}$$

$$(\boldsymbol{V}.\nabla)T = \alpha_{nf}\nabla^2 T \tag{2.3.3}$$

where ρ_{nf} is the density of the nanofluid is, μ_{nf} is dynamic viscosity of the nano fluid and α_{nf} is thermal diffusivity of the nanofluid which are defined as below:

$$\mu_{nf} = \frac{\mu_f}{(1-\phi)^{2.5}}, \qquad \alpha_{nf} = \frac{k_{nf}}{(\rho c_p)_{nf}}, \qquad \rho_{nf} = (1-\phi) + \phi\rho_s$$

$$\left(\rho c_p\right)_{nf} = (1-\phi)\left(\rho c_p\right)_f + \phi\left(\rho c_p\right)_s, \qquad \frac{k_{nf}}{k_f} = \frac{\left(k_s + 2k_f\right) - 2\phi\left(k_f - k_s\right)}{\left(k_s + 2k_f\right) - \phi\left(k_f - k_s\right)}$$

in which ϕ denotes nanoparticles volume fraction, ρ_f and ρ_s densities of base fluids and nano particle material respectively, k_f and $k_s$thermal conductivities of base fluids and nanoparticles respectively, $(\rho c_p)_{nf}$ effective heat capacity of nano fluid and k_{nf} thermal conductivity of nano fluid.

2.3.2 Non-Homogenous Model

It is also called as Buongiorno Model. It is Two-Phase non-homogenous model. In this model concentration equation is also taken in account.

Consider the incompressible fluid flow composed of nanometer-sized metallic particles. The conservation of mass and momentum are given as:

$$\nabla.\boldsymbol{V} = 0 \tag{2.3.4}$$

$$\rho_f\left(\frac{\partial \boldsymbol{V}}{\partial t} + (\nabla.\boldsymbol{V})\boldsymbol{V}\right) = \nabla.\sigma \tag{2.3.5}$$

Where V is the velocity vector, ρ_f is the density of fluid, $\sigma = -pI + \tau$ is the Cauchy stress tensor, $\tau = \mu A_1$ is the extra stress tensor and $A_1 = \nabla \boldsymbol{V} + (\nabla \boldsymbol{V})^T$ is the first Rivlin Erickson tensor. Energy equation in absence of viscous dissipation, Joule heating, heat source/sink and thermal radiation is given by

$$(\rho c)_f \left(\frac{\partial T}{\partial t} + (\boldsymbol{V}.\nabla T) \right) = -\nabla.\boldsymbol{q} + h_s \nabla.\boldsymbol{j_s} \tag{2.3.6}$$

Where $(\rho c)_f$ the effective heat capacity of the base fluid, $\boldsymbol{q}$ is the heat flux, $\boldsymbol{h_s}$ is the specific enthalpy and $\boldsymbol{j_s}$ is the diffusive mass flux of nanoparticle. Following Buongiorno [5] the heat flux $\boldsymbol{q}$ is given by

$$\boldsymbol{q} = -k\nabla T + h_s \boldsymbol{j}_s \; ; \; h_s = c_p T \tag{2.3.7}$$

where k is the thermal conductivity. The diffusive mass flux due to Brownian motion and thermophoresis diffusion is given by

$$\boldsymbol{j}_s = \boldsymbol{j}_{s,B} + \boldsymbol{j}_{s,T} = -\rho_s D_B \nabla C - \rho_s D_T \frac{\nabla T}{T_\infty} \tag{2.3.8}$$

in which D_B is the Brownian diffusion coefficient given by the Einstein–Stokes's equation, and D_T is the thermophoretic diffusion coefficient. Now substituting the expressions for **q** and $\boldsymbol{j}_s$, from equation (2.15) and equation (2.16) we obtain

$$(\rho c)_f \left(\frac{\partial T}{\partial t} + (\boldsymbol{V}.\nabla T)\right) = k\,\nabla^2 T + (\rho c)_s \left(D_B \nabla C.\nabla T + D_T \frac{\nabla T.\nabla T}{T_\infty}\right) \tag{2.3.9}$$

The equation for nanoparticle conservation without chemical reaction and dilute mixture can be written as:

$$\frac{\partial C}{\partial t} + \boldsymbol{V}.\nabla C = -\frac{1}{\rho_s}\nabla.\boldsymbol{j_s} \tag{2.3.10}$$

in which C is the nanoparticle volume fraction, this implies

$$\frac{\partial C}{\partial t} + \boldsymbol{V}.\nabla C = \nabla.\left(D_B \nabla C + D_T \frac{\nabla T}{T_\infty}\right) \tag{2.3.11}$$

2.4 Numerical methods

2.4.1 Keller-box method

The main idea of Keller-box method is writing the governing equations into first order differential system. The "Centered-Difference" derivatives and averages at the midpoints are calculated to get the "finite difference equations. The details of the steps are given below:

2.4.2 The Finite Difference Scheme

We considered the following system of ODE's:

$$H' + 2F = 0 \tag{2.4.1}$$

$$F'' - \frac{1}{B \times Ph}(HF' - F^2 + G^2 - MF - 1) = 0 \tag{2.4.2}$$

$$G'' - \frac{1}{B \times Ph}(HG' - 2FG - MG) = 0 \tag{2.4.3}$$

$$\theta'' - VF \times \Pr(H\theta') = 0 \tag{2.4.4}$$

Where B, VF and Ph are constants.

Introducing new dependent variables $U(x,\eta), V(x,\eta), T(x,\eta)$ so that above equations can be written in the form of first order ODE's:

$$U' - \frac{1}{B \times Ph}(HU - F^2 + G^2 - MF - 1) = 0 \tag{2.4.1a}$$

$$V' - \frac{1}{B \times Ph}(HV - 2FG - MG) = 0 \tag{2.4.2b}$$

$$T' - VF \times \Pr(HT) = 0 \tag{2.4.3c}$$

Now we consider the net points which are defined below:

$$\eta_j = 0, \quad \eta_j = \eta_{j-1} + h_j, \quad j = 1,2,,,J$$

Where h_j is the $\Delta\eta$-spacing. Here j is just sequence of numbers that indicate the coordinate location not tensors or indices.

The derivatives are replaced by the finite difference, for example finite difference form for any points are:

a) $(\quad)_{j-\frac{1}{2}} = \frac{1}{2}\left[(\quad)_{j-1} + (\quad)_j\right]$

b) $\left[\frac{\partial u}{\partial \eta}\right]^{j}_{j-\frac{1}{2}} = \frac{u^{j}_{j-\frac{1}{2}} - u^{j-1}_{j-\frac{1}{2}}}{h_j}$

where for writing the finite difference form of the equations (2.4.1a), (2.4.2b), (2.4.3c) and (2.4.4d) for the mid points $(\eta_{j-1/2})$ using the centered-difference derivatives. This process is called centering about $(x_i, \eta_{j-1/2})$ .We get

$$F' = U \Rightarrow \left(\frac{f_j - f_{j-1}}{h_j}\right) = \frac{1}{2}(U_j - U_{j-1}) \tag{2.4.5}$$

$$G' = V \Rightarrow \left(\frac{g_j - g_{j-1}}{h_j}\right) = \frac{1}{2}(V_j - V_{j-1}) \tag{2.4.6}$$

$$\theta' = W \Rightarrow \left(\frac{\theta_j - \theta_{j-1}}{h_j}\right) = \frac{1}{2}(T_j - T_{j-1}) \tag{2.4.7}$$

Equation (2.4.5 – 2.4.7) are also approximated by centering about $(\eta_{j-1/2})$. And we obtain,

$$-1 - \frac{1}{2}M(F_j + F_{j-1}) - \frac{1}{4}(F_j + F_{j-1})^2 + \frac{1}{4}(G_j + G_{j-1})^2 + \frac{B \times VF(u_j - u_{j-1})}{h_j} - \frac{1}{4}(H_j + H_{j-1})(u_j - u_{j-1}) = 0 \tag{2.4.8}$$

$$\frac{B \times VF(v_j + v_{j-1})}{h_j} - \frac{1}{4}(H_j + H_{j-1})(v_j + v_{j-1}) = 0 \tag{2.4.9}$$

$$\frac{H_j + H_{j-1}}{h_j} = F_j - F_{j-1} \tag{2.4.10}$$

$$\frac{KF(y_j - y_{j-1})}{h_j} - \frac{1}{4}Pr(H_j + H_{j-1})(y_j + y_{j-1}) = 0 \tag{2.4.11}$$

With the boundary conditions

$$F_0 = 1, \qquad G_0 = 0, \qquad H_0 = 0, \qquad y_0 = 1, \tag{2.4.12}$$
$$u_J = 0, \qquad G_J = 1, \qquad T_J = 0$$

2.4.3 Newton's Method

To linearize the nonlinear system of equations using Newton's method. We introduced the following iterates:

$$\begin{aligned} H_j^{k+1} &= H_j^k + \delta H_j^k \\ F_j^{k+1} &= F_j^k + \delta F_j^k \\ U_j^{k+1} &= U_j^k + \delta U_j^k \\ G_j^{k+1} &= G_j^k + \delta G_j^k \\ V_j^{k+1} &= V_j^k + \delta V_j^k \\ T_j^{k+1} &= T_j^k + \delta T_j^k \\ y_j^{k+1} &= y_j^k + \delta y_j^k \end{aligned} \tag{2.4.13}$$

substituting these above expression is in equation (2.4.5 – 2.4.7). This procedure yields the following tridiagonal system:

$$\begin{gathered} a_2\delta F_{j-1} + a_1\delta F_j + a_6\delta G_{j-1} + a_5\delta G_j + a_{10}\delta H_{j-1} + a_9\delta H_j + a_{12}\delta T_{j-1} \\ +a_{11}\delta T_j + a_4\delta u_{j-1} + a_3\delta u_j + a_8\,\delta v_{j-1} + a_7\delta v_j \\ +a_{14}\delta y_{j-1} + a_{13}\delta y_j = r_1 \end{gathered} \tag{2.4.14}$$

$$b_2\delta F_{j-1} + b_1\delta F_j + b_6\,\delta G_{j-1} + b_5\delta G_j + b_{10}\delta H_{j-1} + b_9\delta H_j + b_{12}\delta T_{j-1} + b_{11}\delta T_j + b_4\,\delta u_{j-1} + b_3\delta u_j + b_8\delta v_{j-1} + b_7\delta v_j + b_{14}\delta y_{j-1} + b_{13}\delta y_j = r_2 \quad (2.4.15)$$

$$c_2\delta F_{j-1} + c_1\,\delta F_j + c_6\delta G_{j-1} + c_5\delta G_j + c_{10}\,\delta H_{j-1} + c_9\delta H_j + c_{12}\delta T_{j-1} + c_{11}\delta T_j + c_4\delta u_{j-1} + c_3\,\delta u_j + c_8\delta v_{j-1} + c_7\delta v_j + c_{14}\delta y_{j-1} + c_{13}\delta y_j = r_3 \quad (2.4.16)$$

$$d_2\delta F_{j-1} + d_1\delta F_j + d_6\delta G_{j-1} + d_5\delta G_j + d_{10}\,\delta H_{j-1} + d_9\delta H_j + d_{12}\delta T_{j-1} + d_{11}\delta T_j + d_4\delta u_{j-1} + d_3\delta u_j + d_8\delta v_{j-1} + d_7\,\delta v_j + d_{14}\delta y_{j-1} + d_{13}\delta y_j = r_4 \quad (2.4.17)$$

$$e_2\delta F_{j-1} + e_1\delta F_j + e_6\delta G_{j-1} + e_5\delta G_j + e_{10}\delta H_{j-1} + e_9\delta H_j + e_{12}\delta T_{j-1} + e_{11}\delta T_j + e_4\delta u_{j-1} + e_3\delta u_j + e_8\delta v_{j-1} + e_7\delta v_j + e_{14}\delta y_{j-1} + e_{13}\delta y_j = r_5 \quad (2.4.18)$$

$$f_2\,\delta F_{j-1} + f_1\delta F_j + f_6\delta G_{j-1} + f_5\delta G_j + f_{10}\delta H_{j-1} + f_9\delta H_j + f_{12}\delta T_{j-1} + f_{11}\delta T_j + f_4\delta u_{j-1} + f_3\delta u_j + f_8\delta v_{j-1} + f_7\delta v_j \; f_{14}\delta y_{j-1} + f_{13}\,\delta y_j = r_6 \quad (2.4.19)$$

$$g_2\,\delta F_{j-1} + g_1\delta F_j + g_6\delta G_{j-1} + g_5\delta G_j + g_{10}\delta H_{j-1} + g_9\delta H_j + g_{12}\delta T_{j-1} + g_{12}\,\delta T_j + g_4\,\delta u_{j-1} + g_3\delta u_j + g_8\delta v_{j-1} + g_7\delta v_j + g_{14}\delta y_{j-1} + g_{13}\delta y_j = r_7 \quad (2.4.20)$$

Where the coefficients of above algebraic equations are given below:

$$a_1 = \frac{1}{h_j},$$

$$a_2 = -\frac{1}{h_j},$$

$$a_3 = 0.5,$$

$$a_4 = -0.5,$$

$$a_5 = a_6 = a_7 = a_8 = a_9 = a_{10} = a_{11} = a_{12} = a_{13} = a_{14} = 0\,, \quad (2.4.14a)$$

$$b_1 = b_2 = b_3 = b_4 = 0,$$

$$b_5 = \frac{1}{h_j},$$

$$b_6 = -\frac{1}{h_j},$$

$$b_7 = 0.5,$$

$$b_8 = -0.5,$$

$$b_9 = b_{10} = b_{11} = b_{12} = b_{13} = b_{14} = 0 \qquad (2.4.15b)$$

$$c_1 = c_2 = c_3 = c_4 = c_5 = c_6 = c_7 = c_8 = c_9 = c_{10} = 0,$$

$$c_{11} = \frac{1}{h_j},$$

$$c_{12} = -\frac{1}{h_j},$$

$$c_{13} = 0.5, \qquad (2.4.16c)$$

$$c_{14} = -0.5,$$

$$d_1 = -M - \frac{F_j - F_{j-1}}{2},$$

$$d_2 = -M - \frac{F_j - F_{j-1}}{2},$$

$$d_3 = \frac{B \times VF}{h_j} - \frac{H_j - H_{j-1}}{4},$$

$$d_4 = -4\left(\frac{B \times VF}{h_j}\right) - \frac{H_j - H_{j-1}}{4},$$

$$d_5 = \frac{G_j - G_{j-1}}{2},$$

$$d_6 = \frac{G_j - G_{j-1}}{2},$$

$$d_7 = d_8 = 0,$$

$$d_9 = \frac{U_j - U_{j-1}}{4},$$

$$d_{10} = \frac{U_j - U_{j-1}}{4},$$

$$d_{11} = d_{12} = d_{13} = d_{14} = 0, \quad \text{(2.4.17d)}$$

$$e_1 = \frac{G_j - G_{j-1}}{2},$$

$$e_2 = \frac{G_j - G_{j-1}}{2},$$

$$e_3 = e_4 = 0,$$

$$e_5 = -M - \frac{F_j - F_{j-1}}{2},$$

$$e_6 = -M - \frac{F_j - F_{j-1}}{2},$$

$$e_7 = \frac{B \times VF}{h_j} - \frac{H_j - H_{j-1}}{4},$$

$$e_8 = -4\left(\frac{B \times VF}{h_j}\right) - \frac{H_j - H_{j-1}}{4},$$

$$e_9 = \frac{G_j - G_{j-1}}{4},$$

$$e_{10} = \frac{G_j - G_{j-1}}{4}, \quad \text{(2.4.18e)}$$

$$e_{11} = e_{12} = e_{13} = e_{14} = 0,$$

$$f_1 = 1,$$

$$f_2 = 1,$$

$$f_3 = f_4 = f_5 = f_6 = f_7 = f_8 = 0,$$

$$f_9 = \frac{1}{h_j},$$

$$f_{10} = -\frac{1}{h_j},$$

$$f_{11} = f_{12} = f_{13} = f_{14} = 0 \tag{2.4.19f}$$

$$g_1 = g_2 = g_3 = g_4 = g_5 = g_6 = g_7 = g_8 = 0$$

$$g_9 = -Pr\ \frac{y_j - y_{j-1}}{4},$$

$$g_{10} = -Pr\ \frac{y_j - y_{j-1}}{4},$$

$$g_{11} = g_{12} = 0,$$

$$g_{13} = \frac{KF}{h_j} - Pr\ \frac{H_j - H_{j-1}}{4},$$

$$g_{14} = \frac{-4KF}{h_j} - \Pr\frac{H_j - H_{j-1}}{4} \tag{2.4.20g}$$

$$r_1 = \left(2F_{j-1} - 2F_j + \frac{h_j\left(u_{j-1} + u_j\right)}{2h_j}\right)$$

$$r_2 = \left(2G_{j-1} - G_j + \frac{h_j\left(v_{j-1} + v_j\right)}{2h_j}\right)$$

$$r_3 = \left(2T_{j-1} - T_j + \frac{h_j\left(y_{j-1} + y_j\right)}{2h_j}\right)$$

$$r_4 = \begin{pmatrix} 4 \times B \times VF \times (u_{j-1} - u_j) + h_j(4 + (F_{j-1} + F_j) \\ \times \left((2MF_{j-1} + F_j) - \left(G_{j-1} + G_j\right)2 + \left(H_{j-1} + H_j\right)\left(u_{j-1} + u_j\right)\right)/4h_j \end{pmatrix}$$

$$r_5 = \begin{pmatrix} 4 \times B \times VF \times (v_{j-1} - v_j) + h_j(4 + (F_{j-1} + F_j) \\ \times \left((2MF_{j-1} + F_j) - \left(G_{j-1} + G_j\right)2 + \left(H_{j-1} + H_j\right)\left(v_{j-1} + v_j\right)\right)/4h_j \end{pmatrix}$$

$$r_6 = \left((-h_j \times \left(F_{j-1} + F_j\right) + H_{j-1} - H_j)/h_j\right)$$

$$r_7 = \left(\left(4 \times KF + Prh_j \times H_j + H_{j-1}\right)y_{j-1} + (-4 \times KF + Prh_j\left(H_{j-1} + H_j\right)y_j)/4h_j\right) \tag{2.4.21r}$$

With transformed boundary conditions:

$$\delta F_0 = 1, \qquad \delta G_0 = 0, \qquad \delta H_{\,0} = 0, \qquad \delta y_0 = 1,$$

$$\delta u_J = 0, \qquad \delta G_J = 1, \qquad \delta T_J = 0 \tag{2.4.21}$$

2.4.4 The Block Elimination Method

The linearized differential equation of the system has a block tridiagonal structure. In a vector matrix form it can be written as:

$$\begin{bmatrix} [A_1] & [C_1] & & & & & \\ [B_2] & [A_2] & [C_2] & & & & \\ & & & \ddots & & & \\ & & & \ddots & & & \\ & & & \ddots & & & \\ & & & & [B_{J-1}] & [A_{J-1}] & [C_{J-1}] \\ & & & & & [B_J] & [A_J] \end{bmatrix} \begin{bmatrix} [\delta_1] \\ [\delta_2] \\ \vdots \\ [\delta_{J-1}] \\ [\delta_J] \end{bmatrix} = \begin{bmatrix} [R_1] \\ [R_2] \\ \vdots \\ [R_{J-1}] \\ [R_J] \end{bmatrix}$$

That is:

$$[A][\delta] = [R] \tag{2.4.22}$$

Where the elements of the equation (2.4.22) are given as:

$$[\delta_1] = \begin{bmatrix} \delta u_0 \\ \delta G_0 \\ \delta T_0 \\ \delta F_1 \\ \delta v_1 \\ \delta H_1 \\ \delta y_1 \end{bmatrix}, \; [\delta_J] = \begin{bmatrix} \delta u_{J-1} \\ \delta G_{J-1} \\ \delta T_{J-1} \\ \delta F_J \\ \delta v_J \\ \delta H_J \\ \delta y_J \end{bmatrix}, \qquad 2 \le j \le J \tag{2.4.23}$$

And

$$[R_j] = \begin{bmatrix} (r_1)_j \\ (r_2)_j \\ (r_3)_j \\ (r_4)_j \\ (r_5)_j \\ (r_6)_j \\ (r_7)_j \end{bmatrix} \qquad 1 \le j \le J \tag{2.4.24}$$

To solve the above equation, we suppose A is non-singular matrix and can be solved as:

$$[A] = [L\,|U] \tag{2.4.25}$$

Where

$$[L] = \begin{bmatrix} [\alpha_1] & & & & \\ [B_2] & [\alpha_2] & & & \\ & \ddots & & & \\ & \ddots & & & \\ & & & & [\alpha_{J-1}] \\ & & & [B_J] & [\alpha_J] \end{bmatrix}$$

And

$$[U] = \begin{bmatrix} [I] & [\Gamma_1] & & & & \\ & [I] & [\Gamma_2] & & & \\ & & & \ddots & & \\ & & & \ddots & [I] & [\Gamma_{J-1}] \\ & & & & & [I] \end{bmatrix}$$

Where $[I]$ is the identity matrix of order 5 and $[\alpha_i]$ and $[T_i]$ are 5x5 matrices which elements are determined by following equations:

$$[\alpha_1] = [A_1] \tag{2.4.26}$$

$$[\alpha_1][A_1] = [C_1] \tag{2.4.27}$$

$$[\alpha_j] = [A_j] - [B_j][\Gamma_{j-1}], \qquad j = 2,3 \dots J \tag{2.4.28}$$

$$[\alpha_j][\Gamma_j] = [C_j] \quad j = 2,3 \dots J \tag{2.4.29}$$

Equation (2.4.26) can be substituted into (2.4.27) and we get

$$[L|U|\delta] = [R] \tag{2.4.30}$$

If we define

$$[U|\delta] = [W] \tag{2.4.31}$$

Then equation (2.4.30) becomes

$$[L|W] = [R] \tag{2.4.32}$$

Where

$$W = \begin{bmatrix} W_1 \\ W_2 \\ \vdots \\ W_{J-1} \\ W_J \end{bmatrix},$$

And the $[W_J]$ are the 3x1 matrices. The element W can be solved from equation (2.4.32)

$$[\alpha_1][W_1] = [R_1] \tag{2.4.33}$$

$$[\alpha_j][W_j] = [R_j] - [B_j][W_{j-1}], \qquad 2 \le j \le J \tag{2.4.34}$$

The step in which $\Gamma_j, \alpha_j\, W_j$ are calculated are usually reffered to as the forward step. Once the elements of W are found, equation (2.4.34) then gives the solution δ is so called the backward sweep, in which elements are obtained by following relations:

$$[\delta_J] = [W_J] \tag{2.4.35}$$

$$[\delta_j] = [W_j] - [\Gamma_j][\delta_{j+1}] \qquad 1 \le j \le J-1 \tag{2.4.36}$$

Once the elements of δ are found, equation (2.4.33) can be used to find the (i+1)th iteration in equation (2.4.32). These iterations are repeated until some convergence criterion is satisfied and calculations are stopped when

$$\left|\delta v_0^{(i)}\right| < \varepsilon_1 \tag{2.4.37}$$

where ε_1 is the small prescribed value. For this research work we have considered$\varepsilon_1 = 0.00001$.

Chapter 3 Study of MHD Bodewadt Flow for Casson Nanofluid

3.1 Introduction

This chapter deals with the Bödewadt flow of Casson fluid with water based nanofluid. Three types of nanoparticles namely copper oxide- CuO, Copper-Cu and Silver-Ag are considered for the analysis of flow. Suitable and conventional transformations are applied to the system of equations which resulted in a strong non-linear differential system which is solved by MATLAB Keller Box method.

3.2 Problem formulation

We have adopted the cylindrical coordinates (r, θ, z) such that stationary wall is situated in axial direction i-e $z = 0$. The rotational flow of fluid is generated far from the surface of disk like a rigid body with constant angular velocity Ω. The derivatives along the tangential coordinate θ will be vanished due to axial symmetry of the flow. The flow field is given by the **u** vector whose radial, tangential and axial velocity components are (u, v, w) respectively. The flow is subjected to a constant magnetic field whereas electric field effects are neglected. The Non-Newtonian Casson nanofluid is considered for flow analysis. The fluid is composed of three different types of nanoparticles namely copper oxide – CuO, Copper-Cu and silver– Ag. The fluid temperature is denoted by T and uniform temperature T_w is considered at the disk surface. Far away from the wall the revolving stream is kept at constant temperature T_∞.

The rheological equation of state for an isotropic and incompressible flow of a Casson fluid is given by:

$$\tau_{ij} = \begin{cases} 2\left(\mu_B + \dfrac{p_y}{\sqrt{2\pi}}\right)e_{ij}, & \pi > \pi_c \\ 2\left(\mu_B + \dfrac{p_y}{\sqrt{2\pi_c}}\right)e_{ij}, & \pi < \pi_c \end{cases} \tag{3.1}$$

where $\pi = e_{ij}.e_{ij}$ and e_{ij} are the deformation rate of (i, j) th component, π is the product of deformation rate with itself. π_c is the critical value of π, μ_B is the plastic dynamic viscosity of Casson fluid and p_y is the yield stress of Casson fluid.

By applying the well-known Tiwari and Das model for the transport of nanofluid, the governing equations for conservation of mass, momentum and energy are listed below:

$$\frac{\partial u}{\partial r} + \frac{\partial w}{\partial z} + \frac{u}{r} = 0 \tag{3.1}$$

$$\left(u\,\frac{\partial u}{\partial r} + w\,\frac{\partial u}{\partial z} - \frac{v^2}{r}\right) = -\frac{1}{\rho_{nf}}\frac{\partial p}{\partial r} + \mu_{nf}\left(1+\frac{1}{\beta}\right)\left(\frac{\partial^2 u}{\partial r^2} + \frac{1}{r}\frac{\partial u}{\partial r} + \frac{\partial^2 u}{\partial z^2} - \frac{u}{r^2}\right) - \frac{\sigma B_0^2 u}{\rho_{nf}} \tag{3.2}$$

$$\left(u\,\frac{\partial v}{\partial r} + w\,\frac{\partial v}{\partial z} - \frac{uv}{r}\right) = \mu_{nf}\left(1+\frac{1}{\beta}\right)\left(\frac{\partial^2 v}{\partial r^2} + \frac{1}{r}\frac{\partial v}{\partial r} + \frac{\partial^2 v}{\partial z^2} - \frac{v}{r^2}\right) - \frac{\sigma B_0^2 v}{\rho_{nf}} \tag{3.3}$$

$$\left(u\,\frac{\partial w}{\partial r} + w\,\frac{\partial w}{\partial z}\right) = -\frac{1}{\rho_{nf}}\frac{\partial p}{\partial z} + \mu_{nf}\left(1+\frac{1}{\beta}\right)\left(\frac{\partial^2 w}{\partial r^2} + \frac{1}{r}\frac{\partial w}{\partial r} + \frac{\partial^2 w}{\partial z^2}\right) \tag{3.4}$$

$$u\frac{\partial T}{\partial r} + w\frac{\partial T}{\partial z} = \alpha_{nf}\left(\frac{\partial^2 T}{\partial r^2} + \frac{1}{r}\frac{\partial T}{\partial r} + \frac{\partial^2 T}{\partial z^2}\right) \tag{3.5}$$

The boundary conditions are as under:

$$u = \Omega r, \qquad v = 0, \qquad w = 0\,, \qquad -k\frac{\partial T}{\partial z} = h(T - T_\infty), \quad at\ z = 0$$

$$\frac{\partial u}{\partial z} = 0, \qquad v = \Omega r, \quad T = T_\infty, \quad at\ z \to \infty \tag{3.6}$$

where ρ_{nf} is the density of nano fluid, μ_{nf} dynamic viscosity of nano fluid and α_{nf} is thermal diffusivity of nano fluid which are defined as below:

$$\mu_{nf} = \frac{\mu_f}{(1-\phi)^{2.5}}, \quad \rho_{nf} = (1-\phi) + \phi\rho_s, \qquad \alpha_{nf} = \frac{k_{nf}}{(\rho c_p)_{nf}} \tag{3.7}$$

$$\left(\rho c_p\right)_{nf} = (1-\phi)\left(\rho c_p\right)_f + \phi\left(\rho c_p\right)_s, \quad \frac{k_{nf}}{k_f} = \frac{\left(k_s + 2k_f\right) - 2\phi\left(k_f - k_s\right)}{\left(k_s + 2k_f\right) - \phi\left(k_f - k_s\right)} \tag{3.8}$$

In above mentioned equations ϕ represents the nano particles volume fraction, ρ_f and ρ_s are the densities of base fluids and nanoparticle material respectively. $k_f\ and\ k_s$ denotes the thermal conductivities of base fluids and nano particles respectively, $(\rho c_p)_{nf}$ is the effective heat capacity of nanofluid and k_{nf} is the thermal conductivity of nanofluid.

Both radial pressure and the centrifugal forces are balanced by each other at the frictionless regime and become:

$$\frac{1}{\rho_{nf}}\frac{\partial p}{\partial z} = \Omega r^2 \tag{3.9}$$

Reducing the above mentioned system of equations (3.1) to (3.6) by means of Von Karman's self-similar transformations,

$$\eta = \sqrt{\Omega/\nu_f}\, z, \qquad (u, v, w) = \left(\Omega r F(\eta), \Omega r G(\eta), \sqrt{\frac{\Omega}{\nu_f}} H(\eta) \right)$$

$$(p, T) = \left(2\Omega \mu_f P(\eta), T_\infty + (T_w - T_\infty)\theta(\eta) \right) \tag{3.11}$$

The system is transformed to the following ordinary differential equations with boundary conditions:

$$H' + 2F = 0 \tag{3.12}$$

$$\frac{1}{(1-\phi)^{2.5}(1-\phi\rho_f/\rho_s)}\left(1 + \frac{1}{\beta}\right) F'' - HF' - F^2 + G^2 - MF + 1 = 0 \tag{3.13}$$

$$\frac{1}{(1-\phi)^{2.5}(1-\phi\rho_f/\rho_s)}\left(1 + \frac{1}{\beta}\right) G'' - HG' - 2FG - MG = 0 \tag{3.14}$$

$$\frac{k_{nf}/k_f}{(1+\phi-\phi(\rho c_p)_s/(\rho c_p)_f)} \frac{1}{P_r}\theta'' - H\theta' = 0 \tag{3.15}$$

$$F(0) = C = 1, \qquad G(0) = 0, \qquad H(0) = 0, \qquad \theta'(0) = -Bi\big(1 - \theta(0)\big),$$

$$F'(\infty) = 0, \qquad G(\infty) = 1, \qquad \theta(\infty) = 0 \tag{3.16}$$

In which $P_r = (\mu c)_f/k_f$ is the Prandtl number of the base fluid, $M = B_o^2\, \sigma/\Omega$ is t the Magnetic parameter and $C = ({}^{S}/_{\Omega})$ is the ratio of stretching rate to the rotation rate.

The skin friction coefficient is defined as:

$$C_f = \frac{\sqrt{\tau_r^2 + \tau_\theta^2}}{\rho(r\Omega)^2} \tag{3.17}$$

where the τ_r radial and τ_θ tangential stresses are given by:

$$\tau_r = \mu \frac{\partial u}{\partial z}\Big|_{z=0}, \qquad \tau_\theta = \mu \frac{\partial v}{\partial z}\Big|_{z=0} \tag{3.18}$$

using the transformations (3.11) in equation (3.17) and (3.18), we get

$$\tau_r = r\Omega \sqrt{\frac{\Omega r^2}{\nu_f}} \frac{\mu_f}{(1-\phi)^{2.5}} F'(0), \qquad \tau_\theta = r\Omega \sqrt{\frac{r^2\Omega}{\nu_f}} \frac{\mu_f}{(1-\phi)^{2.5}} G'(0) \tag{3.19}$$

Therefore, skin friction coefficient is calculated and given as:

$$C_f = \sqrt{\frac{\nu_f}{\Omega r^2}} \frac{1}{(1-\phi)^{2.5}} (F'(0)^2 + G'(0)^2)^{1/2} \tag{3.20}$$

The local Nusselt number is defined as:

$$Nu = \frac{r q_w}{k_f (T_w - T_\infty)} \tag{3.21}$$

where q_w is the heat flux from the disk and defined as:

$$q_w = -k_{nf} \frac{\partial T}{\partial z}\Big|_{z=0} \tag{3.22}$$

using variables (3.11) and (3.19) in equation (3.20), we get

$$Nu = -\frac{k_{nf}}{k_f}\sqrt{\frac{r^2\Omega}{v_f}}\,\theta'(0) \tag{3.23}$$

Table 3-1 Thermophysical Properties of base fluid and nanoparticles.

Properties	Base Fluid (Water)	CuO	Cu	Ag
$k\left(^{W}/_{mK}\right)$	0.613	76.5	400	429
$\rho\left(^{kg}/_{m^3}\right)$	997.1	6320	8940	10500
$c_p\left(^{J}/_{kg\ K}\right)$	4179	531.5	385	233

3.3 Numerical results and discussion

To validate our computations, we have made comparison of the numerical results of $H(\infty), c_f\ and - \theta'(0)$ with those of Turkyilmazoglu [14] for the case of regular fluid ($\phi = 0, \beta = 0, M = 0$) (see Table 3.2, 3.3, 3.4). An excellent agreement is seen in all the considered cases.

The axial velocity profile H (η) is demonstrated for different values of ϕ in fig3.1. In this figure all three nanoparticles are shown against the volume fraction. As there is stretching therefore H (η) is negative and the flow is in downward direction near the wall. The behavior of volume fraction of nanoparticle ϕ on the radial component of velocity F (η) is shown in fig 3.2. This velocity profile clearly shows that the flow is moving in radially outward direction in near wall region and is radially inward in far field also increasing volume fraction increases radial velocity. The tangential velocity profile with different values of volume fraction is shown in fig 3.3. This

plot shows an insignificant effect on tangential velocity component G (η) with the volume fraction of nanoparticle. In fig 3.4 temperature profiles for various values of ϕ are plotted.

The fig 3.5 shows the increase in fluid velocity for various values of Casson parameter β. Fig 3.6 presents the velocity profile for the radial component F (η) against the Casson parameter β for Ag-Water. In fig 3.7 negligible velocity effects are seen in the presence of Ag-Water for tangential component G (η).

In fig 3.8 – 3.10 the magnetized behavior of Casson Ag-Water nanofluid are observed. These figures illustrated the increase and decrease of velocities with various values of magnetic parameter M against H(η), F(η) and G(η) respectively. It is worth mentioning that in fig 3.10 we again pointed out that there are negligible Magnus effects on tangential component of velocity G(η).

In fig 3.11 to 3.15 the variation of Prandtl number, volume fraction and Biot numbers are generated on temperature profiles in presence of Ag-Water respectively. These figures pointed out that at high Prandtl number fluid exhibit a weak thermal diffusivity hence it creates a thin thermal boundary layer whereas the high Biot number shows the decrease in heat transfer rate respectively. Moreover, heat transfer rate increase as the volume fraction is increasing.

The fig 3.16 plot demonstrated a non-linear relationship between c_f and ϕ. In fig 3.17-3.19 decrease in velocity at far field against ϕ and β can be seen while it is increasing for M in the vertical direction respectively.

The 3D and 2D streamlines are plotted in fig 3.20 -3.23 for the visualization of fluid flow direction above the surface and far from the disk. These plots illustrate both rotational and stretching effects on the fluid flow. The 2D streamline is plotted in xz-plane.

3.4 Concluding Remarks

1. The axial velocity profiles have a downward direction due to stretching of disk.
2. Casson parameter β and magnetic parameter M have very small effect on radial component of velocity.
3. The boundary layer thickness decreases with the increment of volume fraction of nanoparticles.
4. Thin thermal boundary layer is generated at high Prandtl number.
5. Heat transfer is decreasing against high Prandtl number.
6. There is non-linear relationship between the skin friction coefficient and volume fraction.
7. The temperature profiles show a limiting case of stability at M = 0.08 for both numerical methods.
8. The stretching forces and magnetic forces balance each other therefore direction of flow changes and it start moving in upward direction.

Table 3-2 Numerical values of reduced Nusselt number $Nur = -\theta'(0)$ for Ag-Water with different values of parameters.

ϕ	Bi	C	Pr	β	M	**bvp4c**	**Keller Box**	**Professor Mustafa Turkyilmazoglu [14]**
0.1	1	1	5	1.5	0.1	0.6118	0.6118	
	2					0.8815	0.8815	
	3					1.0333	1.0333	
	4					1.1306	1.1306	
0.1	1	1	5	1.5	0.1	0.6118	0.6118	
			7			0.6666	0.6666	
			10			0.7158	0.7158	
			13			0.7473	0.7473	
0	1	1	5	1.5	0.1	0.6845	0.6845	
0.01						0.6781	0.6781	
0.05						0.6508	0.6508	
0.1						0.6118	0.6118	
0.2						0.5140	0.5140	
0	10000	1	1	100000	0	0.5431	0.5431	0.5431

Table 3-3 Numerical values of skin friction coefficient C_f for Ag-Water with different values of parameters.

ϕ	Bi	C	Pr	β	M	**bvp4c**	**Keller Box**	**Professor Mustafa Turkyilmazoglu [14]**
0.1	1	1	5	0.6	0.1	0.6072	0.6072	
				0.7		0.6074	0.6074	
				0.8		0.6079	0.6079	
				0.9		0.6085	0.6085	
0.1	1	1	5	0.5	0.01	0.6078	0.6078	
					0.02	0.6107	0.6107	
					0.03	0.6136	0.6136	
					0.04	0.6166	0.6166	
0	1	1	5	0.5	0.1	0.6372	0.6372	
0.01						0.6278	0.6278	
0.05						0.6116	0.6116	
0.1						0.6078	0.6078	
0.2						0.6180	0.6180	
0	10000	1	1	100000	0	0.6851	0.6851	0.6851

Table 3-3 Numerical values of H (∞) for Ag-Water with different values of parameters.

ϕ	Bi	C	Pr	β	M	**bvp4c**	**Keller Box**	**Professor Mustafa Turkyilmazoglu [14]**
0.1	1	1	5	0.6	0.1	-0.4520	-0.4520	
				0.7		-0.4267	-0.4267	
				0.8		-0.4069	-0.4069	
				0.9		-0.3910	-0.3910	
0.1	1	1	5	0.5	0.01	-0.4267	-0.4267	
					0.02	-0.3288	-0.3288	
					0.03	-0.2310	-0.2310	
					0.04	-0.1333	-0.1333	
0	1	1	5	0.5	0.1	-0.7176	-0.7176	
0.01						-0.6824	-0.6824	
0.05						-0.5738	-0.5738	
0.1						-0.4856	-0.4856	
0.2						-0.3834	-0.3834	
0	10000	1	1	100000	0	-0.4693	-0.4693	-0.46935

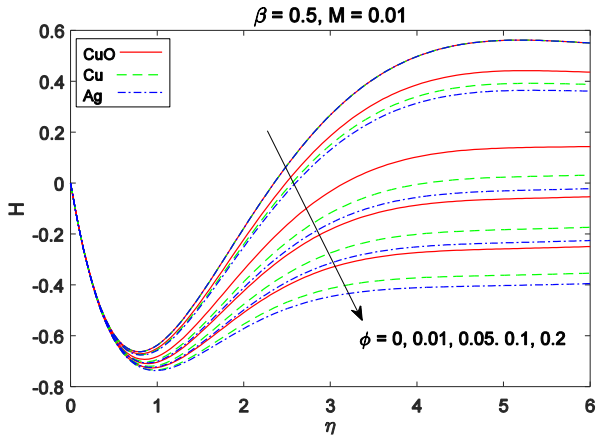

Figure3.1. Effects of ϕ on H

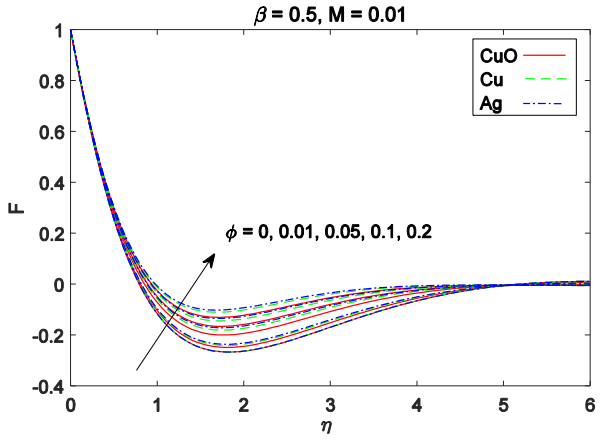

Figure3.2 Effects of ϕ on F

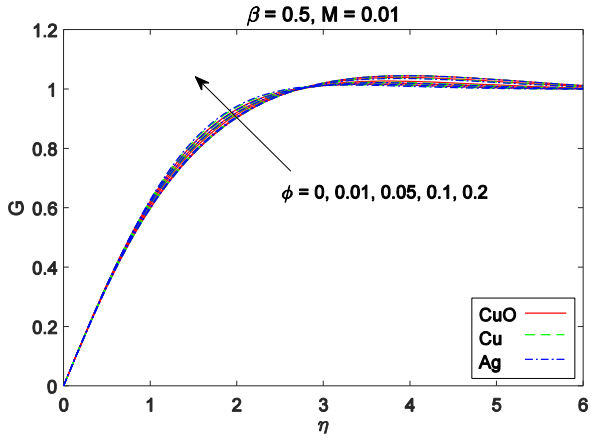

Figure3.3 Effects of ϕ on G

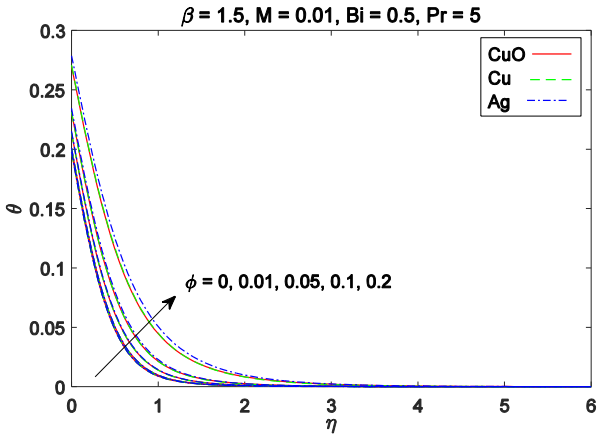

Figure3.4 Effects on ϕ on θ

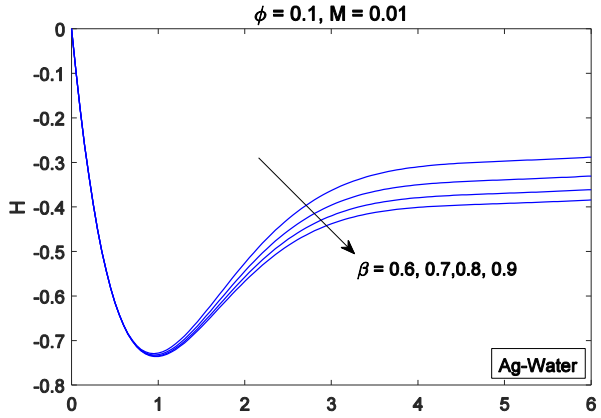

Figure3.5 Effects of β on H

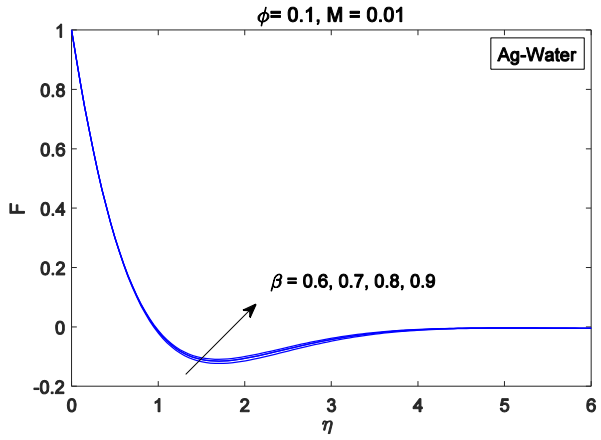

Figure3.6 Effects of β on F

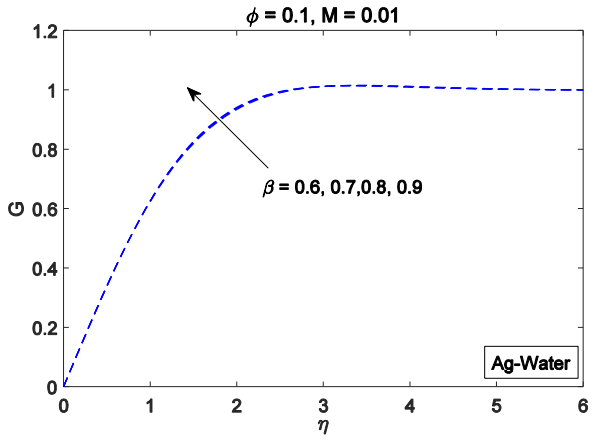

Figure3.7 Effects of β on G

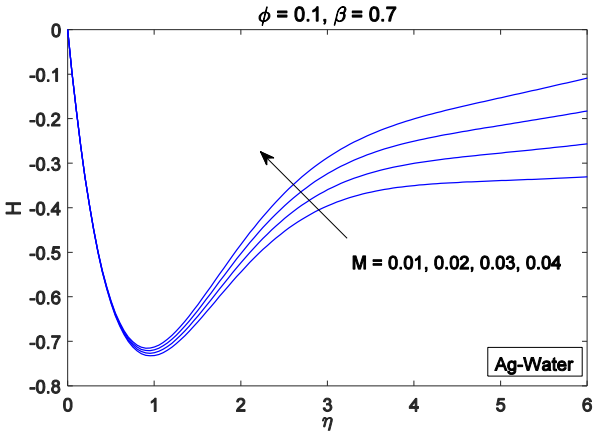

Figure3.8 Effects on M on H

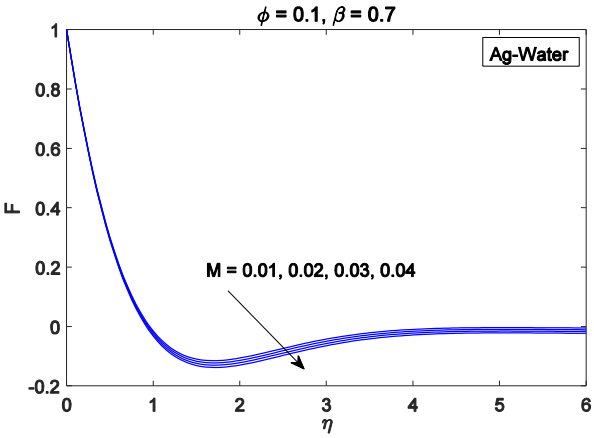

Figure3.9 Effects of M on F

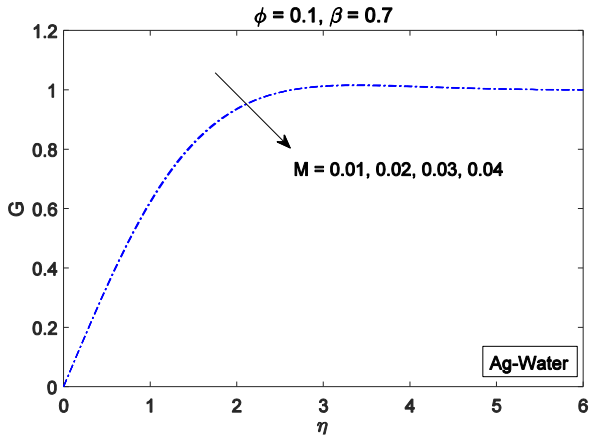

Figure3.10 Effects of M on G

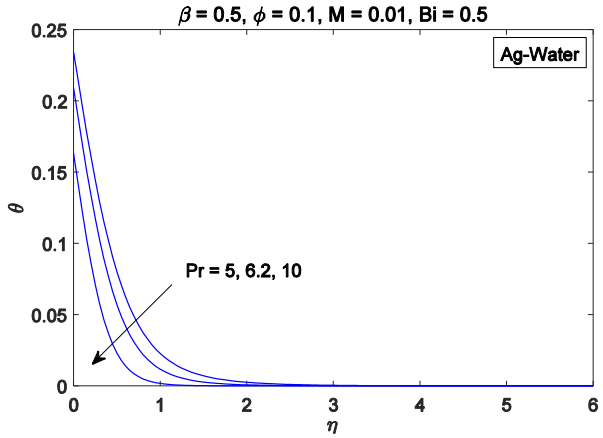

Figure3.11 Effects of Pr on θ

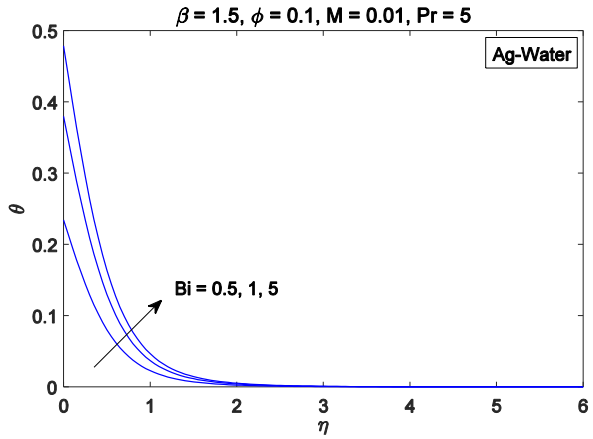

Figure3.12 Effects of Bi on θ

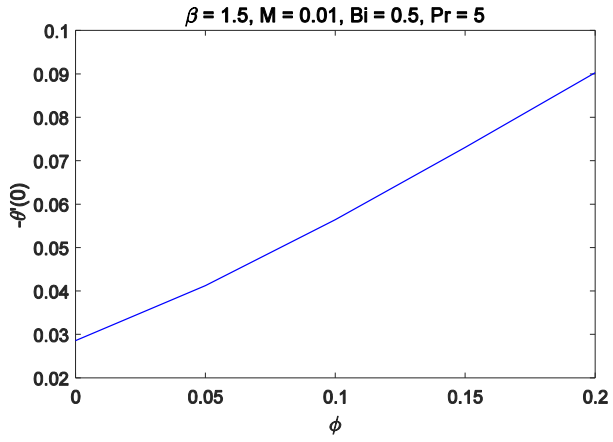

Figure3.13 Effects of ϕ on $-\theta'(0)$

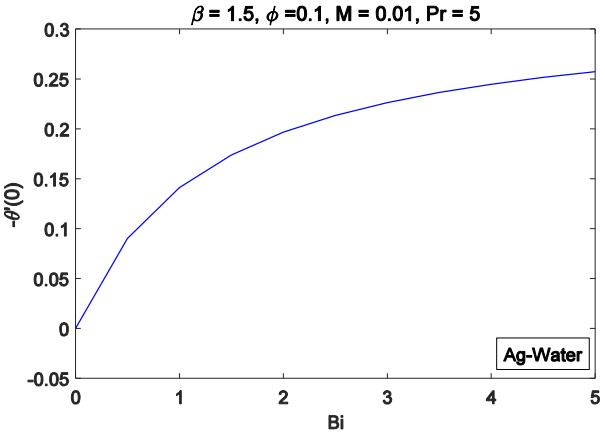

Figure3.14 Effects of Bi on $-\theta'(0)$

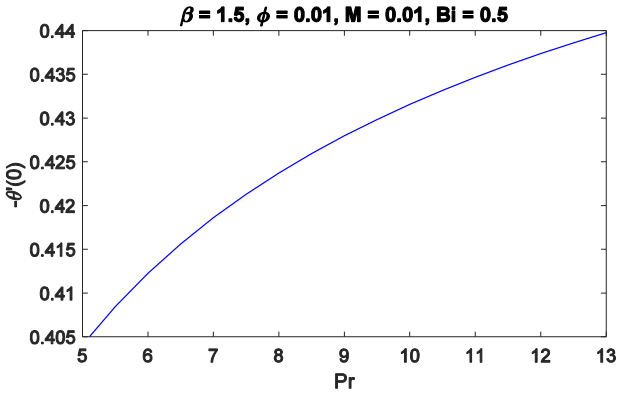

Figure3.15 Effects of Pr on $-\theta'(0)$

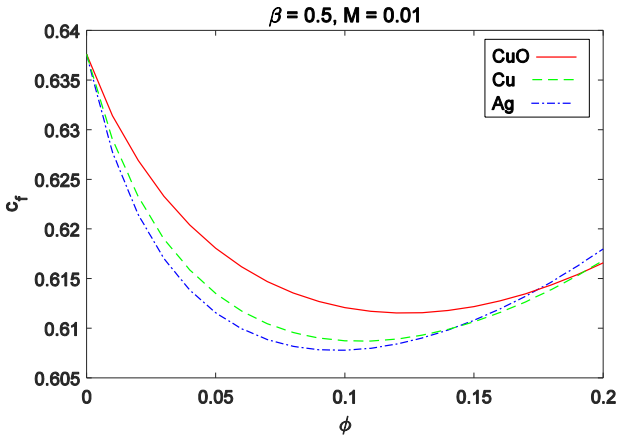

Figure3.16 Effects of ϕ on c_f

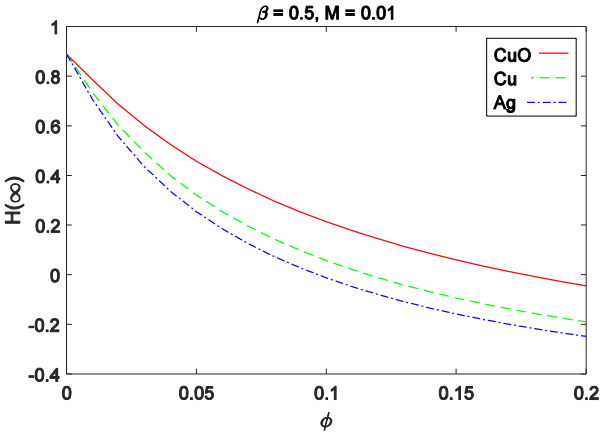

Figure3.17 Effects of ϕ on $H(\infty)$

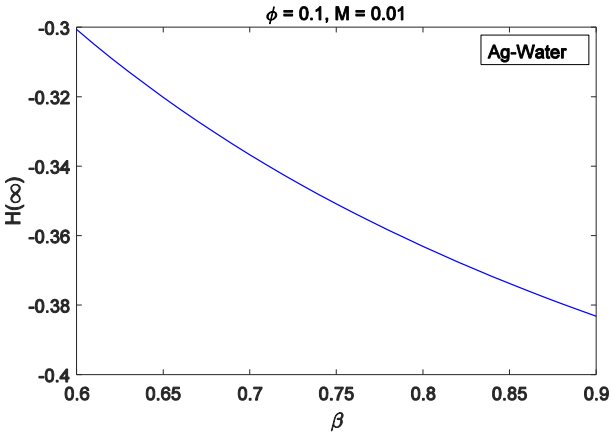

Figure3.18 Effects of β on $H(\infty)$

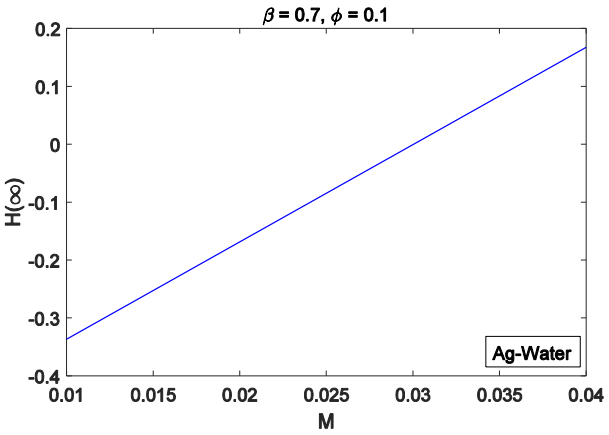

Figure3.19 Effects of M on $H(\infty)$

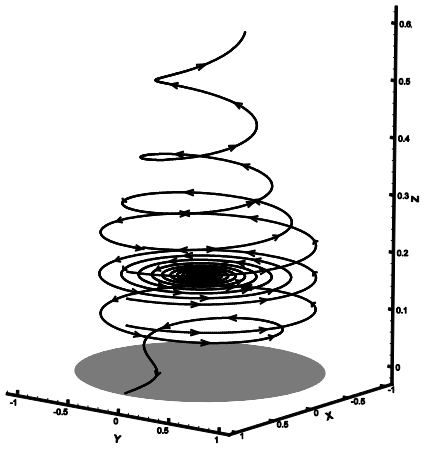

Figure3.20 3D Streamlines for Ag-Water Non-Newtonian Nano fluid when $C = 1, \phi = 0.1, M = 0.08 \; and \; \beta = 1.5$

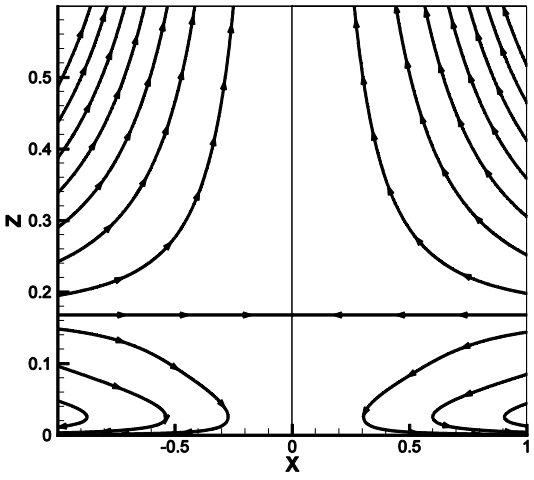

Figure3.21 2D Streamlines for Ag-Water Non-Newtonian Nano fluid when $C = 1, \phi = 0.1, M = 0.08 \; and \; \beta = 1.$

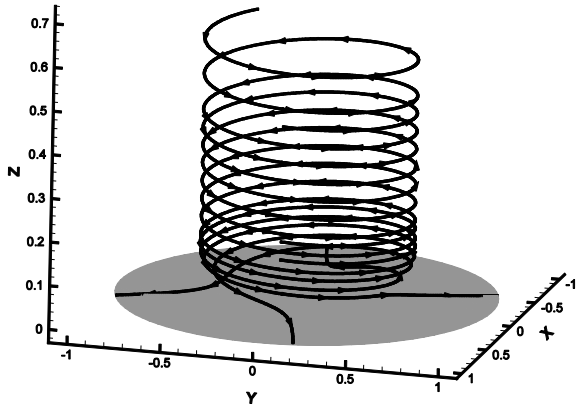

Figure3.22 3D Streamlines for Ag-Water Non-Newtonian Nano fluid when $C = 1, \phi = 0.1, M = 0$ *and* $\beta = 1.5$

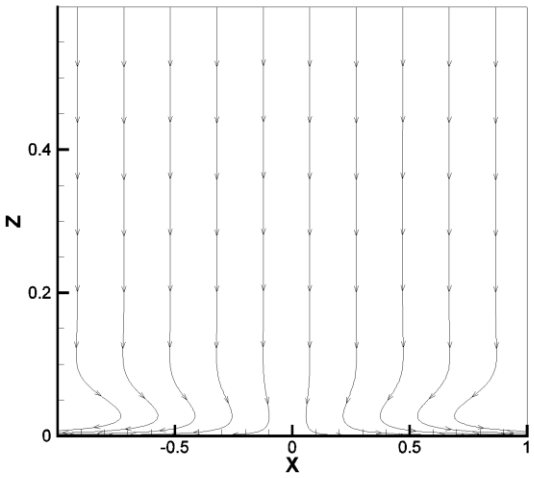

Figure3.23 2D Streamlines for Ag-Water Non-Newtonian Nano fluid when $C = 1, \phi = 0.1, M = 0$ *and* $\beta = 1.5$

Chapter 4 Study of MHD Bödewadt Flow for Casson Nanofluid using Non-Homogenous Model

4.1 Introduction

This chapter explores the Bödewadt flow of nanofluid in the presence of Brownian motion and thermophoresis. Simulations in this study assume that nanoparticle volume fraction at the wall is passively controlled. The relevant boundary layer equations are transformed by appropriate substitutions. Computations are performed by bvp4c Package.

4.2 Problem formulation

We have adopted the cylindrical coordinates (r, θ, z) such that wall situated in axisymmetric direction i.e. $z = 0$. The rotational flow of fluid is generated with constant angular velocity Ω far from the surface of disk where it acts like a rigid body. The derivatives having the tangential component θ will be vanished due to axial symmetry of the flow. The velocity of fluid flow field is given by the **u** vector which represents the radial, tangential and axial velocity components as (u, v, w) respectively. The flow is subjected to a constant magnetic field and electric field is absent. The non-Newtonian Casson nanofluid is considered. The fluid temperature is denoted by T and uniform temperature T_w is considered at the disk surface. The rotational stream far away from the wall is kept at constant temperature T_∞.

The rheological equation of state for an isotropic and incompressible flow of a Casson fluid is given by:

$$\tau_{ij} = \begin{cases} 2\left(\mu_B + \dfrac{p_y}{\sqrt{2\pi}}\right)e_{ij}, & \pi > \pi_c \\ 2\left(\mu_B + \dfrac{p_y}{\sqrt{2\pi_c}}\right)e_{ij}, & \pi < \pi_c \end{cases} \tag{4.1}$$

where $\pi = e_{ij}.e_{ij}$ and e_{ij} are the deformation rate of (i, j)th component, π is the product of deformation rate with itself. π_c is the critical value of π, μ_B is the plastic dynamic viscosity of Casson fluid and p_y is the yield stress of Casson fluid.

Using the velocity field $\boldsymbol{V} = [u(r,z), v(r,z), w(r,z)]$, the temperature distribution $T = T(r,z)$, the magnetic field $B = [0, 0, B_0]$ and nanoparticle volume fraction $C = C(r,z)$ the boundary layer equations for flow with heat and magnetic field transfer in Casson nanofluid are expressed below:

$$\frac{\partial u}{\partial r} + \frac{\partial w}{\partial z} + \frac{u}{r} = 0 \tag{4.2}$$

$$\begin{aligned} &u\,\frac{\partial u}{\partial r} + w\,\frac{\partial u}{\partial z} - \frac{v^2}{r} \\ &= -\frac{1}{\rho}\frac{\partial p}{\partial r} + \nu\left(1 + \frac{1}{\beta}\right)\left(\frac{\partial^2 u}{\partial r^2} + \frac{1}{r}\frac{\partial u}{\partial r} + \frac{\partial^2 u}{\partial z^2} - \frac{u}{r^2}\right) - \frac{\sigma B_0^2 u}{\rho} \end{aligned} \tag{4.3}$$

$$\begin{aligned} &u\,\frac{\partial v}{\partial r} + w\,\frac{\partial v}{\partial z} - \frac{uv}{r} \\ &= \nu\left(1 + \frac{1}{\beta}\right)\left(\frac{\partial^2 v}{\partial r^2} + \frac{1}{r}\frac{\partial v}{\partial r} + \frac{\partial^2 v}{\partial z^2} - \frac{v}{r^2}\right) - \frac{\sigma B_0^2 v}{\rho} \end{aligned} \tag{4.4}$$

$$\begin{aligned} &u\,\frac{\partial w}{\partial r} + w\,\frac{\partial w}{\partial z} \\ &= -\frac{1}{\rho}\frac{\partial p}{\partial z} + \nu\left(1 + \frac{1}{\beta}\right)\left(\frac{\partial^2 w}{\partial r^2} + \frac{1}{r}\frac{\partial w}{\partial r} + \frac{\partial^2 w}{\partial z^2}\right) \end{aligned} \tag{4.5}$$

$$u\frac{\partial T}{\partial r}+w\frac{\partial T}{\partial z}$$
$$=\alpha\left(\frac{\partial^2 T}{\partial r^2}+\frac{1}{r}\frac{\partial T}{\partial r}+\frac{\partial^2 T}{\partial z^2}\right)$$
$$+\Psi\left[D_B\left(\frac{\partial C}{\partial r}\frac{\partial T}{\partial r}+\frac{\partial C}{\partial z}\frac{\partial T}{\partial z}\right)+D_T/T_\infty\left(\left(\frac{\partial T}{\partial z}\right)^2+\left(\frac{\partial C}{\partial z}\right)^2\right)\right] \quad (4.6)$$

$$u\frac{\partial C}{\partial r}+w\frac{\partial C}{\partial z}$$
$$=D_B\left(\frac{\partial^2 C}{\partial r^2}+\frac{1}{r}\frac{\partial C}{\partial r}+\frac{\partial^2 C}{\partial z^2}\right)+D_T/T_\infty\left(\frac{\partial^2 T}{\partial r^2}+\frac{1}{r}\frac{\partial T}{\partial r}+\frac{\partial^2 T}{\partial z^2}\right) \quad (4.7)$$

where u and v are the velocity components along the r- and z- directions respectively, ν is the kinematic viscosity, β= $\mu_B\sqrt{2\pi_c}/p_y$ is Casson fluid parameter, σ is the electricity conductivity, ρ is the fluid density, **α** is the thermal diffusivity, D_B is the Brownian diffusion coefficient, D_T is the thermophoresis diffusion coefficient, T_∞ is the ambient fluid temperature and $\Psi=(\rho c)_p/(\rho c)_f$ is the ratio of effective heat capacity of the nanoparticle material to the effective heat capacity of the fluid. The boundary conditions in the present problem are:

$$u=\Omega r,\qquad v=0,\qquad w=0,\qquad -k\frac{\partial T}{\partial z}=h(T-T_\infty),$$
$$D_B\frac{\partial C}{\partial z}+\frac{D_T}{T_\infty}\frac{\partial T}{\partial z}=0,\quad at\ z=0$$
$$\frac{\partial u}{\partial z}=0,\qquad v=\Omega r,\quad T=T_\infty,\qquad C=C_\infty,\qquad at\ z\to\infty \quad (4.8)$$

The radial pressure and the centrifugal force balance each other at the frictionless regime, hence

$$\frac{1}{\rho_{nf}}\frac{\partial p}{\partial z} = \Omega r^2 \tag{4.9}$$

By means of the Von Karman's self-similar transformations,

$$\eta = \sqrt{\Omega/\nu}\, z, \qquad (u, v, w) = \left(\Omega r F(\eta), \Omega r G(\eta), \sqrt{\frac{\Omega}{\nu}} H(\eta)\right)$$

$$(p, T) = \left(2\Omega\mu_f P(\eta), T_\infty + (T_w - T_\infty)\theta(\eta)\right), \qquad \phi(\eta) = \frac{C - C_\infty}{C_\infty} \tag{4.10}$$

The system is reduced to the following ordinary differential equations:

$$H' + 2F = 0 \tag{4.11}$$

$$\left(1 + \frac{1}{\beta}\right) F'' - HF' - F^2 + G^2 - MF + 1 = 0 \tag{4.12}$$

$$\left(1 + \frac{1}{\beta}\right) G'' - HG' - 2FG - MG = 0 \tag{4.13}$$

$$\frac{1}{P_r}\theta'' - H\theta' + Nb\theta'\phi' + Nt\theta'^2 = 0 \tag{4.14}$$

$$\phi'' - ScH\phi' + \frac{Nt}{Nb}\theta'' = 0 \tag{4.15}$$

$$F(0) = C, \qquad G(0) = 0, \qquad H(0) = 0, \qquad \theta'(0) = -Bi\big(1 - \theta(0)\big),$$

$$Nb\phi'(0) + Nb\theta'(0) = 0$$

$$F'(\infty) = 0, \qquad G(\infty) = 1, \qquad \phi(\infty) = 0, \qquad \theta(\infty) = 0 \tag{4.16}$$

In which $P_r = \frac{\upsilon}{\alpha}$ is the Prandtl number, $M = B_o^2\,\sigma/\Omega$ is t the magnetic parameter, $Nb = \Psi D_B C_\infty/\upsilon$ is the Brownian motion parameter, $Nt = \Psi D_B(T_w - T_\infty)/\upsilon T_\infty$ is the Thermophoresis parameter and $Sc = \upsilon/D_B$ is the Schmidt number and $C = ({}^{S}/_{\Omega})$ is the ratio of stretching rate to the rotation rate.

The skin friction coefficient is defined as:

$$C_f = \frac{\sqrt{\tau_r^2 + \tau_\theta^2}}{\rho(r\Omega)^2} \tag{4.17}$$

where the τ_r radial and τ_θ tangential stresses are given by:

$$\tau_r = \mu \frac{\partial u}{\partial z}\Big|_{z=0}, \qquad \tau_\theta = \mu \frac{\partial v}{\partial z}\Big|_{z=0} \tag{4.18}$$

where μ is the dynamic viscosity, using (4.9) in (4.16) and (4.17) we get,

$$\tau_r = \mu \sqrt{\frac{\Omega r^2}{\nu}} F'(0), \qquad \tau_\theta = \mu \sqrt{\frac{r^2\Omega}{\nu}}\, G'(0) \tag{4.19}$$

$$C_f = \sqrt{\frac{\nu}{\Omega r^2}}\, (F'(0)^2 + G'(0)^2)^{1/2} \tag{4.20}$$

Using the Fourier law of heat conduction, we get the local Nusselt number, which is defined as:

$$Nu = \frac{rq''}{k(T_w - T_\infty)} \tag{4.21}$$

where q'' the heat flux is defined as:

$$q'' = -k\frac{\partial T}{\partial z}\Big|_{z=0} + c_p T\left[D_B\frac{\partial C}{\partial z}\Big|_{z=0} + \frac{D_T}{T_\infty}\frac{\partial T}{\partial z}\Big|_{z=0}\right] \tag{4.22}$$

using equations (4.8), (4.20) and (4.21) we obtained,

$$Nu = -\sqrt{\frac{r^2\Omega}{\nu}}\,\theta'(0). \tag{4.23}$$

and

$$Sh = -\sqrt{\frac{r^2\Omega}{\nu}}\,\phi'(0). \tag{4.24}$$

4.3 Numerical results and discussion

In fig 4.1-4.3 the effects of Casson parameter are shown. In these plots we can see for H(η) and G(η) there is increase of velocity whereas for F(η) there is decrease in velocity. It is happening because of the stretching of sheet. In fig 4.4-4.6 we are analyzing the magnetized effects on the velocities. Here it is worth noticing that there are negligible effects on the tangential component of velocity G(η) and very small effects can be seen on radial component of velocity.

In fig 4.7-4.9 we have plotted temperature profiles for different parameters. In these plots we have observed for higher values of Prandtl number there is weak thermal diffusivity hence thin thermal boundary layer is generated. While there is decrease in heat transfer rate layer for high thermophoresis parameter Nt. Moreover, we can see decrease of temperature against the Biot number as well.

In fig 4.10 and 4.11 the impacts of various parameters are plotted for concentration profiles of the flow. We can see that there is decrease in concentration against the Sc. While there is increase in thermophoresis parameter Nt.

The variations against Nusselt number are plotted in fig 4.12-4.14. We can observe the decrease in heat transfer rate with increase in Pr and increase in heat transfer rate with Bi. While there is decrease in heat transfer rate layer for high thermophoresis parameter Nt. The effects on the Skin friction coefficient are illustrated in fig 4.15 and 4.16. We can clearly see that it is increasing against Casson parameter β and magnetic parameter M. While results for $\phi'(0)$ are also computed against Nt and Sc in fig 4.17and 4.18 respectively. It shows the increase and decrease trend for Nt and Sc. The fluid flow pattern for H(∞) is observed in fig 4.19 and 4.20 for Casson and magnetic parameters which shows an increasing trend.

4.4 Concluding Remarks

1. Brownian motion has negligible effect on temperature and heat transfer profiles.
2. Thermal boundary layer decreases with increase in thermophoresis parameter.
3. At high thermophoresis parameter there is a decrease in heat transfer rate.

4. The temperature profiles show a limiting case of stability at M = 0.08 for both numerical methods.

Table 4-1 Numerical values of Nusselt number with different values of parameters.

C	β	M	Pr	Bi	Sc	Nt	**bvp4c**
1	0.7	0.01	1	1	5	0.5	0.4853
			5				-0.7893
			7				-0.8312
			10				-0.8680
1	0.7	0.01	5	0.5	5	0.5	-0.4441
				1			-0.8312
				5			-3.3247
1	0.7	0.01	5	1	5	0.1	-2.2124
						0.5	-2.2124
						0.9	-3.7960

Table 4-2 Numerical values of Sherwood number $\phi'(0)$ with different values of parameters.

C	β	M	Pr	Bi	Sc	Nt	**bvp4c**
1	0.7	0.01	7	1	5	0.5	0.8312
					10		0.8285
					15		0.8265
1	0.7	0.01	7	1	5	0.1	0.1521
						0.5	0.8312
						0.9	1.5610

Table 4-3 Numerical values of skin friction coefficient with different values of parameters.

C	β	M	Pr	Bi	Sc	Nt	**bvp4c**
1	0.5	0.01	7	1	5	0.5	0.6033
	0.6						0.6125
	0.7						0.6187
	0.8						0.6228
1		0.01	7	1	5	0.5	0.6033
		0.02					0.6046
		0.03					0.6058
		0.04					0.6071

Table 4-4 Numerical values of H (∞) with different values of parameters.

C	β	M	Pr	Bi	Sc	Nt	**bvp4c**
1	0.5	0.01	7	1	5	0.5	-0.5504
	0.6						-0.3484
	0.7						-0.4000
	0.8						-0.3904
1		0	7	1	5	0.5	-0.6906
		0.01					-0.5504
		0.02					-0.2986
		0.03					-0.3646
		0.04					-0.4281
		0.05					0.0305

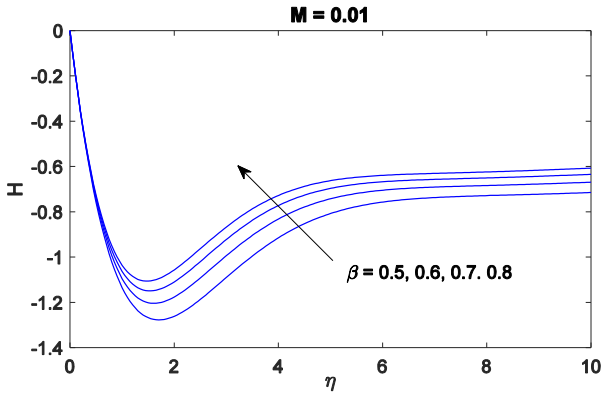

Figure 4.1 Effects of β on H

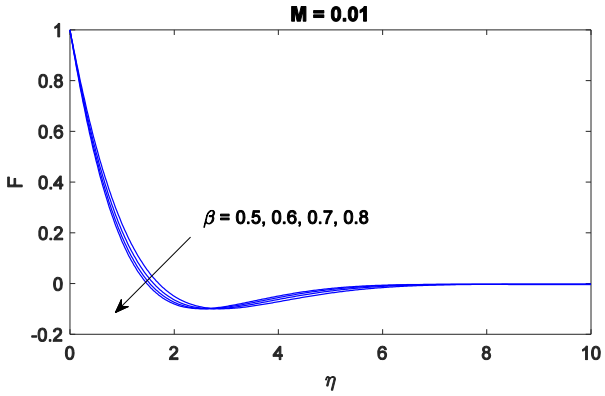

Figure 4.2 Effects of β on F

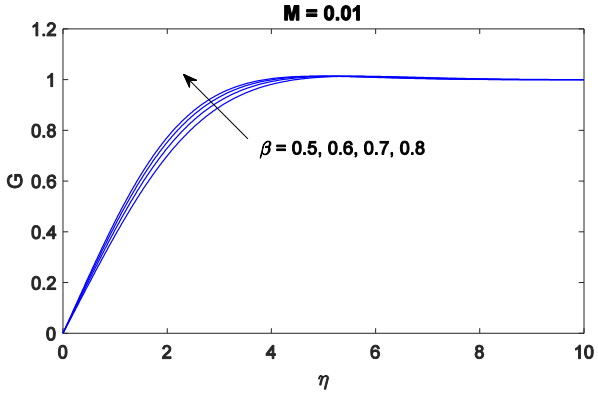

Figure 4.3 Effects of β on G

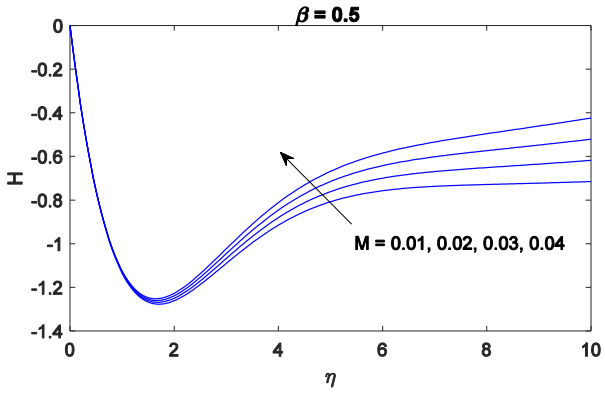

Figure 4.4 Effects of M on H

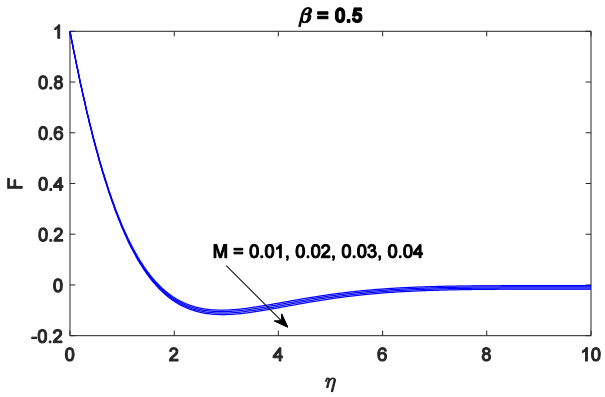

Figure 4.5 Effects of M on F

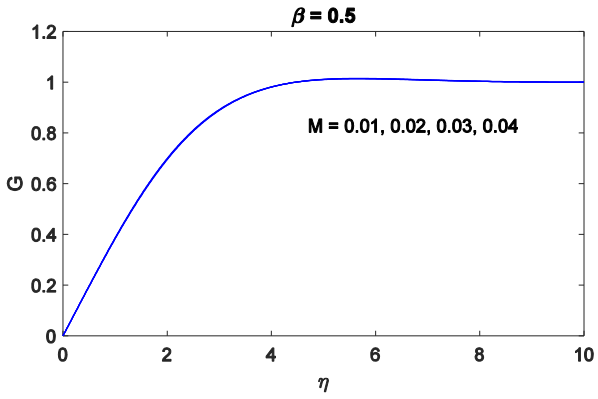

Figure 4.6 Effects of M on G

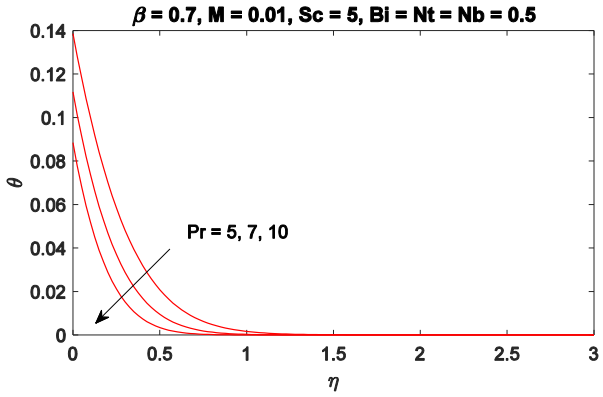

Figure 4.7 Effects of Pr on θ

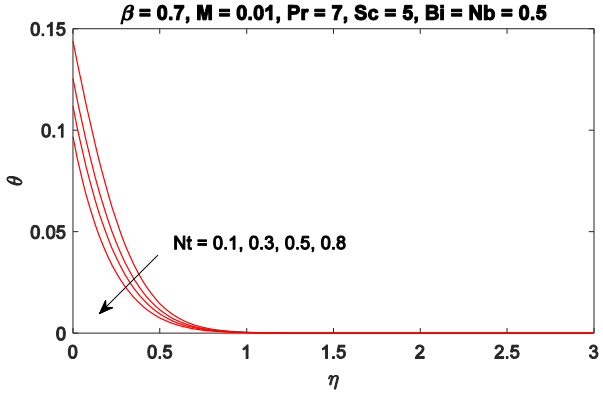

Figure 4.8 Effects of Nt on θ

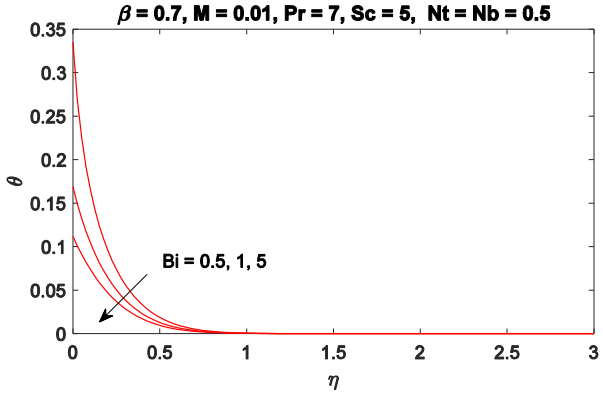

Figure 4.9 Effects of Bi on θ

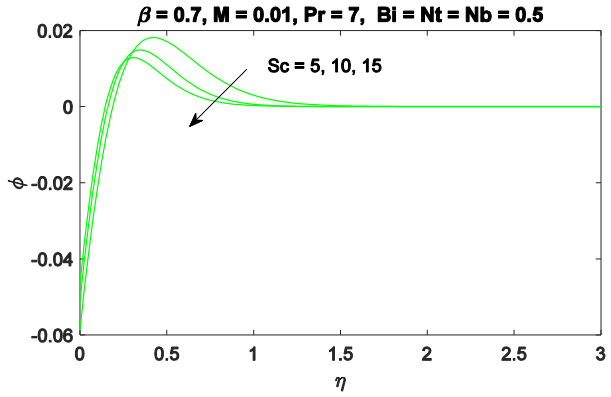

Figure 4.10 Effects of Sc on ϕ

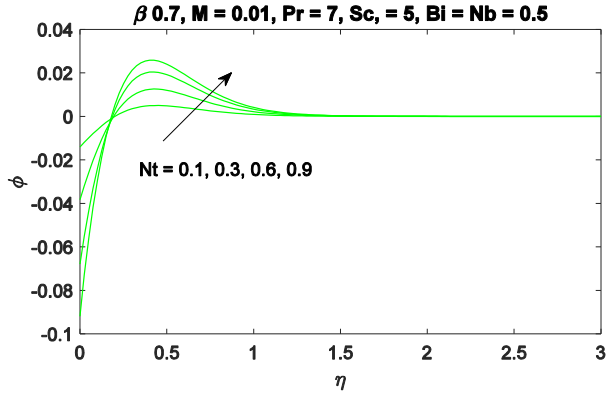

Figure 4.11 Effects of Nt on ϕ

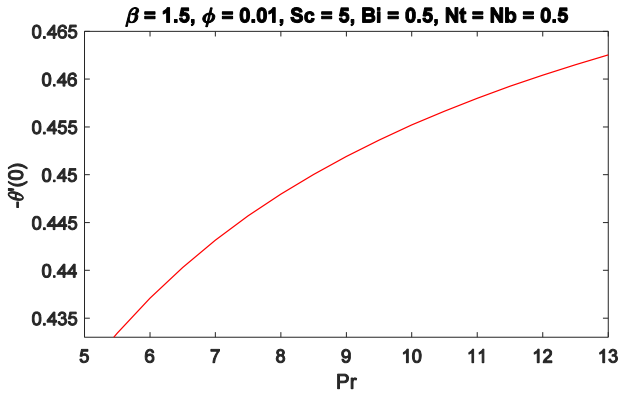

Figure 4.12 Effects of Pr on $-\theta'(0)$

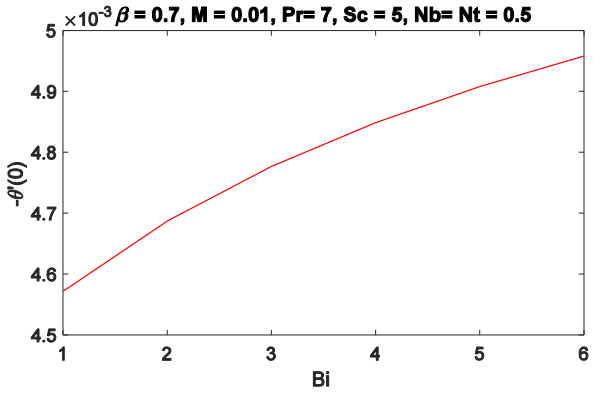

Figure 4.13 Effects of Bi on $-\theta'(0)$

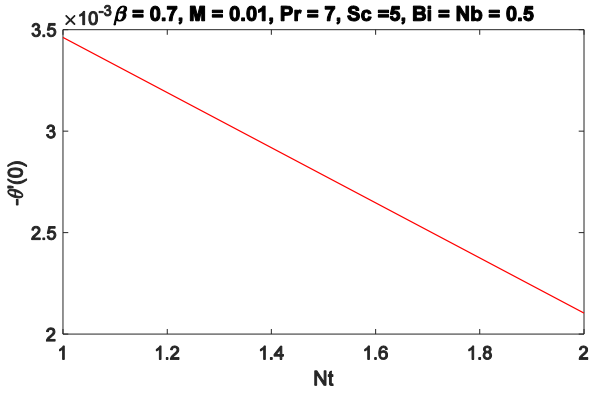

Figure 4.14 Effects of Nt on $-\theta'(0)$

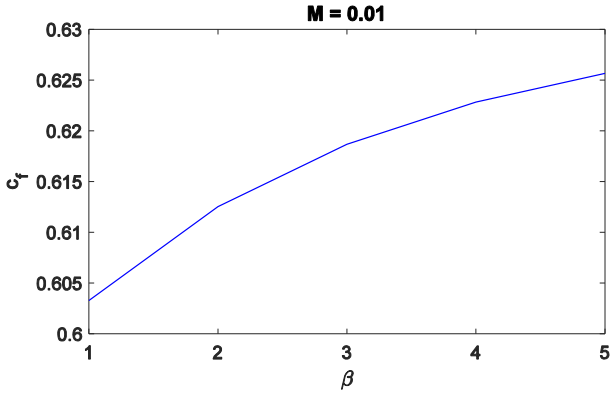

Figure 4.15 Effects of β on c_f

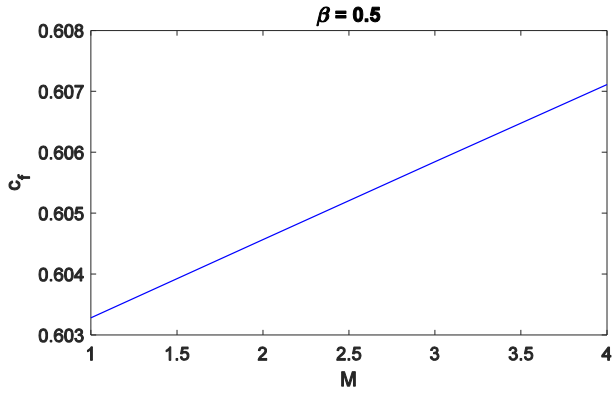

Figure 4.16 Effects of M on c_f

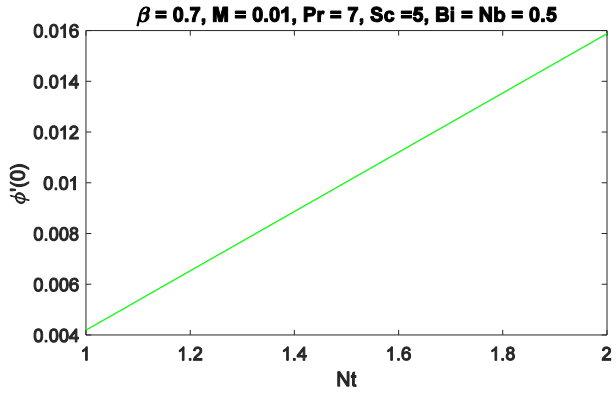

Figure 4.17 Effects of Nt on $\phi'(0)$

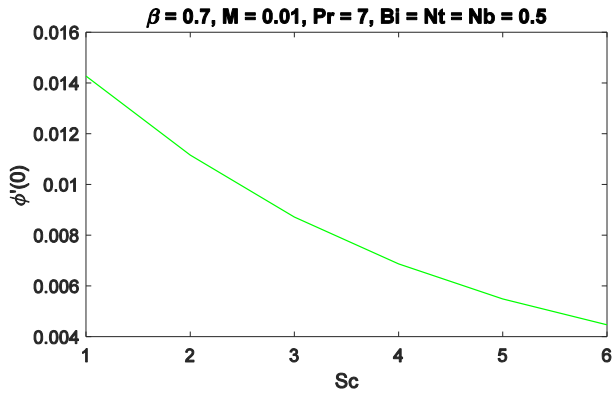

Figure 4.18 Effects of Sc on $\phi'(0)$

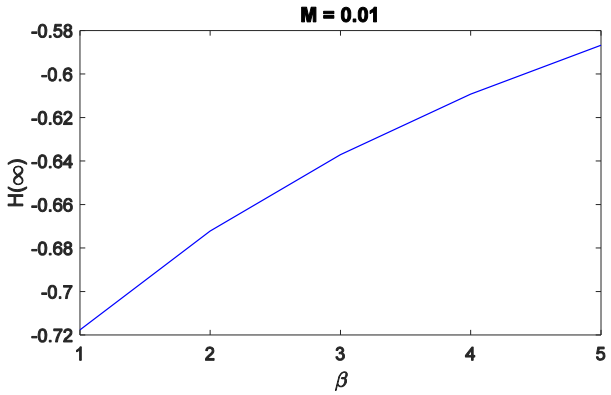

Figure 4.19 Effects of β on H (∞)

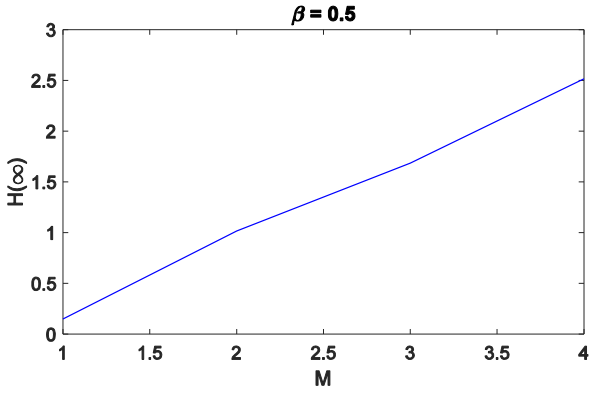

Figure 4.20 Effects of M on H (∞)

Chapter 5 Conclusion and Future Work Suggestions

5.1 Conclusion

Study of rotating flows for Casson nanofluid under uniform magnetic field has been carried out. The flow analysis through graphs and 3D images have been examined and discussed. The following conclusions are drawn from the current work:

1. The axial velocity profiles have a downward direction due to stretching of disk.
2. Casson parameter β and magnetic parameter M have very small effect on radial component of velocity.
3. The boundary layer thickness decreases with the increment of volume fraction of nanoparticles.
4. Thin thermal boundary layer is generated at high Prandtl number.
5. There is non-linear relationship between the skin friction coefficient and volume fraction.
6. The temperature profiles exhibit a limiting case of stability at M = 0.08 for both numerical methods.
7. The stretching forces and magnetic forces balance each other therefore direction of flow changes and it start moving in upward direction Brownian motion has negligible effect on temperature and heat transfer profiles.
8. At high thermophoresis parameter there is a decrease in heat transfer rate.
9. Thermal boundary layer decrease with increase in Nt.

5.2 Recommendations for Future Work

1. The same work can be done with unsteady fluid flow.
2. Different Non-Newtonian fluids models such as Maxwell fluid model, Jaffery fluid model, Bingham Model, Bird-Carreau model, Cross-Power law model, Herschel-Bulkey model, second-grade model etc. can also be considered to make flow analysis for the current work.
3. Thermal radiation effects can be also examined for the same fluid flow problem.
4. Hybrid nanofluid transport model can also be applied on the current problem.
5. Cattaneo–Christov heat flux model can also applicable on the current problem.
6. Linear and non-linear stretching effects can also be considered.

References

1. Masuda, H., Ebata, A. and Teramae, K., 1993. Alteration of thermal conductivity and viscosity of liquid by dispersing ultra-fine particles. Dispersion of Al2O3, SiO2 and TiO2 ultra-fine particles. *Journal: NETSU BUSSEI **1993**, Volume 7, Number 4; Page(s) 227 To 233.*
2. Choi, S.U. and Eastman, J.A., 1995. Enhancing thermal conductivity of fluids with nanoparticles (No. ANL/MSD/CP-84938; CONF-951135-29). *Argonne National Lab., IL (United States).*
3. Eastman, J.A., Choi, S.U.S., Li, S., Yu, W. and Thompson, L.J., 2001. Anomalously increased effective thermal conductivities of ethylene glycol-based nanofluids containing copper nanoparticles. *Applied physics letters*, *78*(6), pp.718-720.
4. Buongiorno, J., 2006. Convective transport in nanofluids. *Journal of heat transfer*, *128*(3), pp.240-250.
5. Tiwari, R.K. and Das, M.K., 2007. Heat transfer augmentation in a two-sided lid-driven differentially heated square cavity utilizing nanofluids. *International Journal of heat and Mass transfer*, *50*(9-10), pp.2002-2018.
6. Wang, C.Y., 1988. Stretching a surface in a rotating fluid. *Zeitschrift für angewandte Mathematik und Physik ZAMP*, *39(2), pp.177-185.*
7. Rajeswari, V. and Nath, G., 1992. Unsteady flow over a stretching surface in a rotating fluid. *International Journal of Engineering Science*, *30*(6), pp.747-756.
8. Nazar, R., Amin, N. and Pop, I., 2004. Unsteady boundary layer flow due to a stretching surface in a rotating fluid. *Mechanics Research Communications*, *31*(1), pp.121-128.

9. Hayat, T., Javed, T. and Sajid, M., 2008. Analytic solution for MHD rotating flow of a second grade fluid over a shrinking surface. *Physics Letters A*, *372*(18), pp.3264-3273.
10. Abbas, Z., Javed, T., Sajid, M. and Ali, N., 2010. Unsteady MHD flow and heat transfer on a stretching sheet in a rotating fluid. *Journal of the Taiwan Institute of Chemical Engineers*, *41*(6), pp.644-650.
11. Batchelor, G.K., 1951. Note on a class of solutions of the Navier-Stokes equations representing steady rotationally-symmetric flow. *The quarterly journal of mechanics and applied mathematics*, *4*(1), pp.29-41.
12. Evans, D.J., 1969. The rotationally symmetric flow of a viscous fluid in the presence of an infinite rotating disc with uniform suction. *The Quarterly Journal of Mechanics and Applied Mathematics*, *22*(4), pp.467-485.
13. McLeod, J.B., 1970. A note on rotationally symmetric flow above an infinite rotating disc. *Mathematika*, *17*(2), pp.243-249.
14. Turkyilmazoglu, M., 2015. Bödewadt flow and heat transfer over a stretching stationary disk. *International Journal of Mechanical Sciences*, *90*, pp.246-250.
15. Griffiths, P.T., Garrett, S.J. and Stephen, S.O., 2014. The neutral curve for stationary disturbances in rotating disk flow for power-law fluids. *Journal of Non-Newtonian Fluid Mechanics*, *213*, pp.73-81.
16. Mustafa, M., Khan, J.A., Hayat, T. and Alsaedi, A., 2015. On Bödewadt flow and heat transfer of nanofluids over a stretching stationary disk. *Journal of Molecular Liquids*, *211*, pp.119-125.

17. Sheikholeslami, M., Hatami, M. and Ganji, D.D., 2015. Numerical investigation of nanofluid spraying on an inclined rotating disk for cooling process. *Journal of Molecular Liquids*, *211*, pp.577-583.
18. Xun, S., Zhao, J., Zheng, L., Chen, X. and Zhang, X., 2016. Flow and heat transfer of Ostwald-de Waele fluid over a variable thickness rotating disk with index decreasing. *International Journal of Heat and Mass Transfer*, *103*, pp.1214-1224.
19. Latiff, N.A., Uddin, M.J. and Ismail, A.M., 2016. Stefan blowing effect on bioconvective flow of nanofluid over a solid rotating stretchable disk. *Propulsion and Power Research*, *5*(4), pp.267-278.
20. Ming, C., Zheng, L., Zhang, X., Liu, F. and Anh, V., 2016. Flow and heat transfer of power-law fluid over a rotating disk with generalized diffusion. *International Communications in Heat and Mass Transfer*, *79*, pp.81-88.
21. Imtiaz, M., Hayat, T., Alsaedi, A. and Asghar, S., 2017. Slip flow by a variable thickness rotating disk subject to magnetohydrodynamics. *Results in Physics*, *7*, pp.503-509.
22. Doh, D.H. and Muthtamilselvan, M., 2017. Thermophoretic particle deposition on magnetohydrodynamic flow of micropolar fluid due to a rotating disk. *International Journal of Mechanical Sciences*, *130*, pp.350-359.
23. Hayat, T., Rashid, M., Imtiaz, M. and Alsaedi, A., 2017. Nanofluid flow due to rotating disk with variable thickness and homogeneous-heterogeneous reactions. *International Journal of Heat and Mass Transfer*, *113*, pp.96-105.

24. Devi, M.C., Rajendran, L., Yousaf, A.B. and Fernandez, C., 2017. Non-linear differential equations and rotating disc electrodes: Padé approximationtechnique. *Electrochimica Acta*, *243*, pp.1-6.
25. Guha, A. and Sengupta, S., 2017. Non-linear interaction of buoyancy with von Kármán's swirling flow in mixed convection above a heated rotating disc. *International Journal of Heat and Mass Transfer*, *108*, pp.402-416.
26. Ellahi, R., Zeeshan, A., Hussain, F. and Abbas, T., 2018. Study of shiny film coating on multi-fluid flows of a rotating disk suspended with nano-sized silver and gold particles: A comparative analysis. *Coatings*, *8*(12), p.422.
27. Babu, M.S., Gangadhar, K. and Lavanya, M., 2017. MHD boundary layer flow of Casson nanofluid over a vertical exponentially stretching cylinder under Newtonian heating. *Research Journal of Pharmacy and Technology*, *10*(4), p.998.
28. Sarojamma, G. and Vendabai, K., 2015. Boundary layer flow of a casson nanofluid past a vertical exponentially stretching cylinder in the presence of a transverse magnetic field with internal heat generation/absorption. *Int. J. Mech. Aerospace, Industrial, Mechatronic and Manufacturing Engineering*, *9*, pp.1-10.
29. Hussain, T., Shehzad, S.A., Alsaedi, A., Hayat, T. and Ramzan, M., 2015. Flow of Casson nanofluid with viscous dissipation and convective conditions: a mathematical model. *Journal of Central South University*, *22*(3), pp.1132-1140.
30. Kumar, P.S. and Gangadhar, K., 2015. Effect of chemical reaction on slip flow of MHD Casson fluid over a stretching sheet with heat and mass transfer. *Adv. Appl. Sci. Res*, *6*(8), pp.205-223.

31. Mustafa, M. and Khan, J.A., 2015. Model for flow of Casson nanofluid past a non-linearly stretching sheet considering magnetic field effects. *AIP Advances*, *5*(7), p.077148.
32. Mustafa, M., Hayat, T., Pop, I. and Aziz, A., 2011. Unsteady boundary layer flow of a Casson fluid due to an impulsively started moving flat plate. *Heat Transfer—Asian Research*, *40*(6), pp.563-576.
33. Nadeem, S., Haq, R.U. and Lee, C., 2012. MHD flow of a Casson fluid over an exponentially shrinking sheet. *Scientia Iranica*, *19*(6), pp.1550-1553.
34. Mustafa, M., Hayat, T., Ioan, P. and Hendi, A., 2012. Stagnation-point flow and heat transfer of a Casson fluid towards a stretching sheet. *Zeitschrift für Naturforschung A*, *67*(1-2), pp.70-76.
35. Mukhopadhyay, S., 2013. Casson fluid flow and heat transfer over a nonlinearly stretching surface. *Chinese Physics B*, *22*(7), p.074701.
36. Mukhopadhyay, S., Moindal, I.C. and Hayat, T., 2014. MHD boundary layer flow of Casson fluid passing through an exponentially stretching permeable surface with thermal radiation. *Chinese Physics B*, *23*(10), p.104701.
37. Mustafa, M. and Khan, J.A., 2015. Model for flow of Casson nanofluid past a non-linearly stretching sheet considering magnetic field effects. *AIP Advances*, *5*(7), p.077148.
38. Ramesh, K. and Devakar, M., 2015. Some analytical solutions for flows of Casson fluid with slip boundary conditions. *Ain Shams Engineering Journal*, *6*(3), pp.967-975.

39. Sandeep, N., Koriko, O.K. and Animasaun, I.L., 2016. Modified kinematic viscosity model for 3D-Casson fluid flow within boundary layer formed on a surface at absolute zero. *Journal of Molecular Liquids*, *221*, pp.1197-1206.
40. Qing, J., Bhatti, M., Abbas, M., Rashidi, M. and Ali, M., 2016. Entropy generation on MHD Casson nanofluid flow over a porous stretching/shrinking surface. *Entropy*, *18*(4), p.123.
41. Ali, M.E. and Sandeep, N., 2017. Cattaneo-Christov model for radiative heat transfer of magnetohydrodynamic Casson-ferrofluid: a numerical study. *Results in physics*, *7*, pp.21-30.
42. Reddy, J.R., Sugunamma, V. and Sandeep, N., 2017. Enhanced heat transfers in the flow of dissipative non-Newtonian Casson fluid flow over a convectively heated upper surface of a paraboloid of revolution. *Journal of Molecular Liquids*, *229*, pp.380-388.
43. Rehman, K.U., Malik, A.A., Malik, M.Y., Sandeep, N. and Saba, N.U., 2017. Numerical study of double stratification in Casson fluid flow in the presence of mixed convection and chemical reaction. *Results in physics*, *7*, pp.2997-3006.
44. Kumaran, G. and Sandeep, N., 2017. Thermophoresis and Brownian moment effects on parabolic flow of MHD Casson and Williamson fluids with cross diffusion. *Journal of Molecular Liquids*, *233*, pp.262-269.
45. Ali, F., Sheikh, N.A., Khan, I. and Saqib, M., 2017. Magnetic field effect on blood flow of Casson fluid in axisymmetric cylindrical tube: A fractional model. *Journal of Magnetism and Magnetic Materials*, *423*, pp.327-336.

46. Raju, C.S.K., Hoque, M.M. and Sivasankar, T., 2017. Radiative flow of Casson fluid over a moving wedge filled with gyrotactic microorganisms. *Advanced Powder Technology*, *28*(2), pp.575-583.
47. Uddin, M.J., Bég, O.A. and Amin, N., 2014. Hydromagnetic transport phenomena from a stretching or shrinking nonlinear nanomaterial sheet with Navier slip and convective heating: a model for bio-nano-materials processing. *Journal of Magnetism and Magnetic Materials*, *368*, pp.252-261.
48. Lin, Y., Zheng, L., Zhang, X., Ma, L. and Chen, G., 2015. MHD pseudo-plastic nanofluid unsteady flow and heat transfer in a finite thin film over stretching surface with internal heat generation. *International Journal of Heat and Mass Transfer*, *84*, pp.903-911.
49. Sheikholeslami, M., Rashidi, M.M., Hayat, T. and Ganji, D.D., 2016. Free convection of magnetic nanofluid considering MFD viscosity effect. *Journal of Molecular Liquids*, *218*, pp.393-399.
50. Abbasi, F.M., Shehzad, S.A., Hayat, T. and Ahmad, B., 2016. Doubly stratified mixed convection flow of Maxwell nanofluid with heat generation/absorption. *Journal of Magnetism and Magnetic Materials*, *404*, pp.159-165.
51. Hayat, T., Muhammad, T., Shehzad, S.A. and Alsaedi, A., 2016. On three-dimensional boundary layer flow of Sisko nanofluid with magnetic field effects. *Advanced Powder Technology*, *27*(2), pp.504-512.
52. Heysiattalab, S., Malvandi, A. and Ganji, D.D., 2016. Anisotropic behavior of magnetic nanofluids (MNFs) at filmwise condensation over a vertical plate in

presence of a uniform variable-directional magnetic field. *Journal of Molecular Liquids*, *219*, pp.875-882.

53. Hayat, T., Aziz, A., Muhammad, T. and Alsaedi, A., 2016. On magnetohydrodynamic three-dimensional flow of nanofluid over a convectively heated nonlinear stretching surface. *International Journal of Heat and Mass Transfer*, *100*, pp.566-572.
54. Hayat, T., Waqas, M., Khan, M.I. and Alsaedi, A., 2016. Analysis of thixotropic nanomaterial in a doubly stratified medium considering magnetic field effects. *International Journal of Heat and Mass Transfer*, *102*, pp.1123-1129.
55. Malvandi, A., Ghasemi, A. and Ganji, D.D., 2016. Thermal performance analysis of hydromagnetic Al2O3-water nanofluid flows inside a concentric microannulus considering nanoparticle migration and asymmetric heating. *International Journal of Thermal Sciences*, *109*, pp.10-22.